(A)

Evx1as interaction propensities

	Binding
MLL1	
SET domain	(moderate) 38
CXXC domain	(high) 74
PHD domain	(moderate) 43
Ash1	
SET domain	(high) 93
PHD domain	(absent) 0
Wdr5	(low) 25
Cfp1	(high) 98

HOTTIP interaction propensities

	Binding
MLL1	
SET domain	(moderate) 64
CXXC domain	(high) 90
PHD domain	(low) 43
Ash1	
SET domain	(high) 93
PHD domain	(modertate) 36
Wdr5	(high) 84
Cfp1	(high) 99

(B)

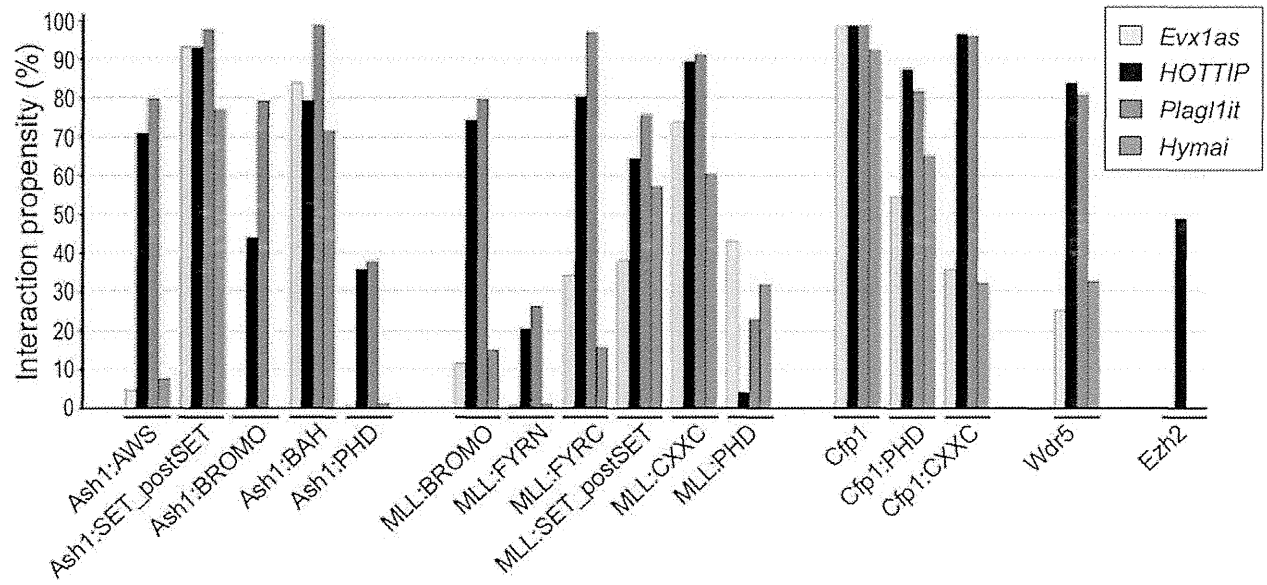

(C)

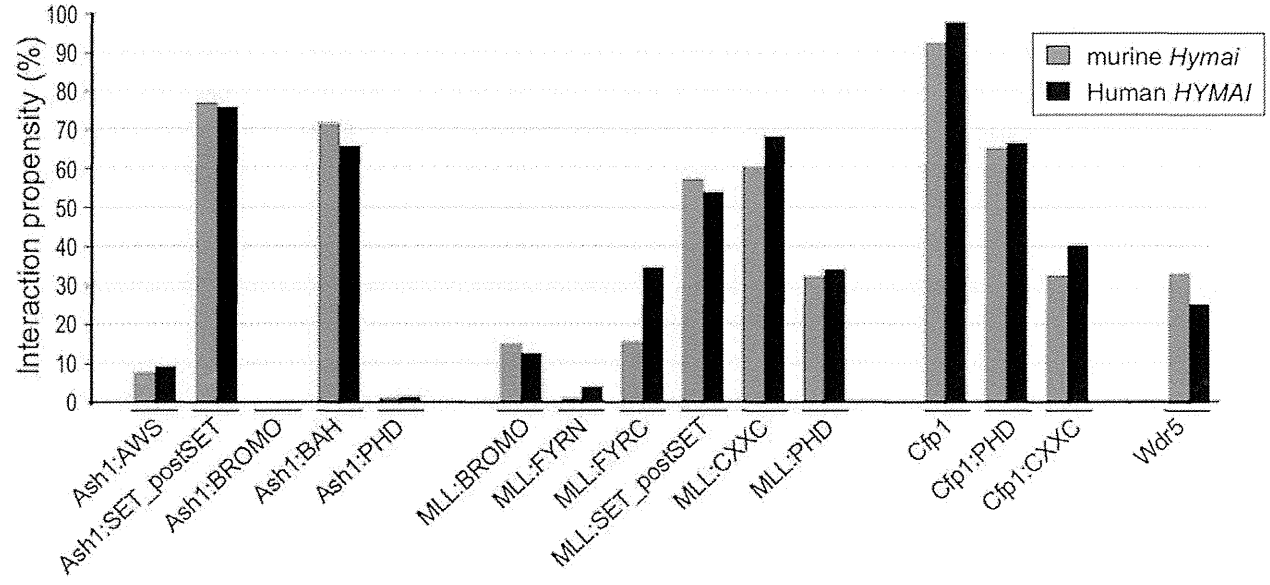

Figure 4. CatRAPID analysis of ncRNA-protein interactions. (A) CatRAPID analysis reveals the interaction propensities of the control ncRNAs; *Evx1as* with MLL1/KTM2A and *HOTTIP* with WDR5. (B) The interaction propensities for the control ncRNAs and for *Hymai* and *Plagl1it* with various components (and sub-domains) of the H3K4 and H3K27 methylation machinery. (C) Similar ncRNA-protein interactions revealed by CatRAPID analysis for *Hymai* (in black) and the human orthologue *HYMAI* (in red).
doi:10.1371/journal.pone.0038907.g004

tions. The PCR products were subcloned into pGEM T-easy vector (Promega) and 20 colonies were sequenced using an ABI prism 3100 DNA sequencer (Applied Biosystems). The full-length sequences of Plagl1it and Hymai have been deposited in GenBank and have been assigned the accession numbers JN595789 and JN595790 respectively.

Northern Blot Analysis

To determine the size of *Plagl1it*, *Hymai* and the truncated *Plagl1* transcripts, we used custom-made northern blots containing 20 μg of total RNA extracted from CD1 embryos (Zyagen, San Diego, USA). The blots were hybridised with an *β-Actin* probe prior to use to confirm equal loading. Unique sequences for each transcript were amplified by PCR, and the resulting amplicon probes were radiolabelled with (^{32}P)CTP using the Ready-To-Go DNA labelling Beads (Amersham). Hybridizations were carried out overnight at 65°C and washed according to manufacturer's instructions.

RT-PCR Conditions

Allelic RT-PCRs, reactions were performed using primers that flanked polymorphisms. The amplification cycle numbers for each transcript were determined to be within the exponential phase of the PCR, which varied for each gene, but was between 32–42 cycles. The subsequent amplicons were sequenced using both the forward and reverse primers (Table S1 for primer sequences).

Real-time RT-PCR

All PCR amplifications were run in triplicate on a 7900 Fast real-time PCR machine (Applied Biosystems) following the manufacturers' protocol. All primers were optimized using SYBR Green (see additional data file 5 for primer sequences) and melt curve analysis to ensure that amplicons were specific and free of primer-dimer products. Thermal cycle parameters included Taq polymerase activation at 95°C for 10 min for 1 cycle, repetitive denaturation at 95°C for 15 sec, and annealing at 60°C for 1 min for 40 cycles. All resulting triplicate cycle threshold (Ct) values had to be with 1 Ct of each other. The quantitative values for each triplicate were determined as a ratio with the level of *Gapdh* expression (B-actin for actinomycin experiments), which was measured in the same sample, and then averaged to provide relative expression values.

Analysis of Allelic DNA-methylation

Approximately 1 μg DNA was subjected to sodium bisulphite treatment and purified using the EZ GOLD methylation kit (ZYMO, Orange, CA). Bisulphite PCR primers for each region were used with Hotstar Taq polymerase (Qiagen, West Sussex, UK) at 40 cycles and the resulting PCR product cloned into pGEM-T easy vector (Promega) for subsequent sequencing (see Table S1 for primer sequences).

Chromatin Immunoprecipitation (ChIP)

ChIP was carried out on wild type embryos, MEF cells and *Dnmt3l* −/+ embryos. ChIP was performed as previously described [6] using the following Upstate Biotechnology antisera directed against H3ac (06-599), H3K9ac (07-352), H3K4me2 (07-030), H3K9me3 (060904589), H3K27me3 (07-449) and H4K20me3 (07-463) (Upstate Biotechnology). DNA extracted from precipitated chromatin fractions was PCR amplified, and parental alleles were discriminated by either SSCP (*PLAGL1*-DMR) or by direct sequencing. Polymorphisms within 1 kb of the CpG islands were identified by interrogating SNP databases or through genomic sequencing (see Table S1 for primer sequences and location). Only ChIP sample sets that showed enrichment for additional imprinting control regions were used in the analysis. Precipitation levels in the ChIP samples were determined by real-time PCR amplification, using SYBR Green PCR kit (Applied Biosystems). Each PCR was run in triplicate and results are presented as percentage precipitation and normalised to the level of the *H19*-DMD, since methylation at this paternally methylated DMR is unaffected after maternal transmission of the Dnmt3l deleted allele.

catRAPID Analysis

We employed the catRAPID algorithm to predict potential interactions between ncRNAs and proteins [16]. This algorithm was trained using RNA-protein pairs described in the NPInter database. We calculated the average interaction propensity of each RNA species (fragmented into ~1 kb segments because of sequence length restrictions) against complete protein and unique functional domains. Multiple domains adjacent in sequence were joined together (e.g. three PHD domains in MLL1 and SET/proSET regions). In the case of domain association with a size <50 amino acids additional flanking amino acids were added upstream and downstream.

Supporting Information

Figure S1 (**A**) Expression of *Plagl1*, *Hymai* and *Plagl1it* in various tissues from embryos at different gestational stages (e = embryonic day; NB = new born). (**B**) Northern blot analysis using probes specific for *Plagl1* exon 2–3, *Plagl1it* and *Hymai*. A single transcript of less than 4 kb is detected for *Plagl1it* consistent with RACE and RT-PCRs results. Truncated *Plagl1* transcripts, between 700–1.7 kb, correspond to CJ065374 and AI607573.
(TIF)

Figure S2 Mapping of the RACE products to determine the extents of the novel transcripts and open reading frame analysis. (A) The overlapping start sites for P1-*Plagl1* and *Hymai*. (B) analysis for open reading frame using DNA Strider for *Hymai*. (C and D) The 5′ and 3′ ends of *Plagl1it* in relation to *Plagl1* transcripts, and ORF analysis.
(TIF)

Figure S3 Chromatin immunoprecipitation of WDR5 in MEF cells. (A) The upper panel shows PCR amplification of the β-actin promoter control region and *Plagl1*-DMR in the WDR5-ChIP. The lower panel is the genotypes of the input and IP (B x C), showing preferential precipitation of the paternal allele compared to input as calculated from relative area under the nucleotide curve at the SNP position. (B) Confirmation of preferential paternal enrichment by *Hinf*1 RFLP analysis.
(TIF)

Table S1 Table of PCR primer sequences.
(DOC)

Acknowledgments

We are grateful to Humberto Ferreira for help and advice with northern blots, and thank Valeria Romanelli for critical reading of the manuscript.

URLs.

http://igc.otago.ac.nz/home.html.

Author Contributions

Conceived and designed the experiments: IIP GT PA DM. Performed the experiments: IIP AMT DC FC AGA CC PA DM. Analyzed the data: IIP FC DC PA DM. Contributed reagents/materials/analysis tools: DB KH RF GT. Wrote the paper: IIP AMT DC FC AGA CC DB KH RF GT PA DM.

References

1. Reik W, Walter J (2001) Genomic imprinting: parental influence on the genome. Nat Rev Genet 2: 21–32.
2. Tomizawa S, Kobayashi H, Watanabe T, Andrews S, Hata K, et al. (2011) Dynamic stage-specific changes in imprinted differentially methylated regions during early mammalian development and prevalence of non-CpG methylation in oocytes. Development 5: 811–820.
3. Bourc'his D, Xu GL, Lin CS, Bollman B, Bestor TH (2003) Dnmt3L and the establishment of maternal genomic imprints. Science 21: 2536–2539.
4. Hata K, Okano M, Lei H, Li E (2002) Dnmt3L cooperates with the Dnmt3 family of de novo DNA methyltransferases to establish maternal imprints in mice. Development 129: 1983–1993.
5. Kaneda M, Okano M, Hata K, Sado T, Tsujimoto N, et al. (2004) Essential role for de novo DNA methyltransferase Dnmt3a in paternal and maternal imprinting. Nature 24: 900–903.
6. Henckel A, Nakabayashi K, Sanz LA, Feil R, Hata K, et al. (2009) Histone methylation is mechanistically linked to DNA methylation at imprinting control regions in mammals. Hum Mol Genet 18: 3375–3383.
7. Nagano T, Mitchell JA, Sanz LA, Pauler FM, Ferguson-Smith AC, et al. (2008) The Air noncoding RNA epigenetically silences transcription by targeting G9a to chromatin. Science 322: 1717–1720.
8. Pandey RR, Mondal T, Mohammad F, Enroth S, Redrup L, et al. (2008) Kcnq1ot1 antisense noncoding RNA mediates lineage-specific transcriptional silencing through chromatin-level regulation. Mol Cell 32: 232–246.
9. Kamiya M, Judson H, Okazaki Y, Kusakabe M, Muramatsu M, et al. (2000) The cell cycle control gene ZAC/PLAGL1 is imprinted–a strong candidate gene for transient neonatal diabetes. Hum Mol Genet. 9: 453–460.
10. Smith RJ, Arnaud P, Konfortova G, Dean WL, Beechey CV, et al. (2002) The mouse Zac1 locus: basis for imprinting and comparison with human ZAC. Gene 292: 101–112.
11. Abdollahi A (2007) LOT1 (ZAC1/PLAGL1) and its family members: mechanisms and functions. J Cell Physiol 210: 16–25.
12. Abdollahi A, Pisarcik D, Roberts D, Weinstein J, Cairnns P, et al. (2003) LOT1 (PLAGL1/ZAC1), the candidate tumor suppressor gene at chromosome 6q24–25, is epigenetically regulated in cancer. J Biol Chem. 2 278: 6041–6049.
13. Mackay DJ, Coupe AM, Shield JP, Storr JN, Temple IK, et al. (2002) Relaxation of imprinted expression of ZAC and HYMAI in a patient with transient neonatal diabetes mellitus. Hum Genet. 110: 139–144.
14. Mackay DJ, Temple IK (2010) Transient neonatal diabetes mellitus type 1. Am J Med Genet C Semin Med Genet.154C: 335–342.
15. Seidl CI, Stricker SH, Barlow DP (2006) The imprinted Air ncRNA is an atypical RNAPII transcript that evades splicing and escapes nuclear export. EMBO J. 25: 3565–3575.
16. Bellucci M, Agostini F, Masin M, Tartaglia GG (2011) Predicting protein associations with long noncoding RNAs. Nat Methods. 8: 444–445.
17. Dinger ME, Amaral PP, Mercer TR, Pang KC, Bruce SJ, et al. (2008) Long noncoding RNAs in mouse embryonic stem cell pluripotency and differentiation. Genome Res. 18: 1433–1445.
18. Wang KC, Yang YW, Liu B, Sanyal A, Corces-Zimmerman R, et al. (2011) A long noncoding RNA maintains active chromatin to coordinate homeotic gene expression. Nature 472: 120–124.
19. Arima T, Wake N (2006) Establishment of the primary imprint of the HYMAI/PLAGL1 imprint control region during oogenesis. Cytogenet Genome Res. 113: 247–252.
20. Valleley EM, Cordery SF, Bonthron DT (2007) Tissue-specific imprinting of the ZAC/PLAGL1 tumour suppressor gene results from variable utilization of monoallelic and biallelic promoters. Hum Mol Genet. 16: 972–981.
21. Chotalia M, Smallwood SA, Ruf N, Dawson C, Lucifero D, et al. (2009) Transcription is required for establishment of germline methylation marks at imprinted genes. Genes Dev. 23: 105–117.
22. Mattick JS, Makunin IV (2006) Non-coding RNA. Hum Mol Genet. 15 Spec No1: R17–29.
23. Fuke H, Ohno M (2008) Role of poly (A) tail as an identity element for mRNA nuclear export. Nucleic Acids Res. 36: 1037–1049.
24. Carmody SR, Wente SR (2009) mRNA nuclear export at a glance. J Cell Sci. 122: 1933–1937.
25. Zhao J, Ohsumi TK, Kung JT, Ogawa Y, Grau DJ, et al. (2010) Genome-wide identification of polycomb-associated RNAs by RIP-seq. Mol Cell. 40: 939–953.
26. Ørom UA, Derrien T, Beringer M, Gumireddy K, Gardini A, et al. (2010) Long noncoding RNAs with enhancer-like function in human cells. Cell 143: 46–58.
27. Krajewski WA, Nakamura T, Mazo A, Canaani E (2005) A motif within SET-domain proteins binds single-stranded nucleic acids and transcribed and supercoiled DNAs and can interfere with assembly of nucleosomes. Mol Cell Biol. 25: 1891–1899.
28. Hall TM (2005) Multiple modes of RNA recognition by zinc finger proteins. Curr Opin Struct Biol. 15: 367–373.
29. Arima T, Drewell RA, Arney KL, Inoue J, Makita Y, et al. (2001) A conserved imprinting control region at the HYMAI/ZAC domain is implicated in transient neonatal diabetes mellitus. Hum Mol Genet. 10: 1475–1483.
30. Monk D (2010) Deciphering the cancer imprintome. Brief Funct Genomics. 9: 329–339.

CLINICAL REPORT

AMERICAN JOURNAL OF medical genetics PART A

Aberrant Methylation of H19-DMR Acquired After Implantation Was Dissimilar in Soma Versus Placenta of Patients With Beckwith–Wiedemann Syndrome

Ken Higashimoto,[1] Kazuhiko Nakabayashi,[2] Hitomi Yatsuki,[1] Hokuto Yoshinaga,[1] Kosuke Jozaki,[1] Junichiro Okada,[3] Yoriko Watanabe,[3] Aiko Aoki,[4] Arihiro Shiozaki,[4] Shigeru Saito,[4] Kayoko Koide,[1] Tsunehiro Mukai,[5] Kenichiro Hata,[2] and Hidenobu Soejima[1]*

[1]Division of Molecular Genetics & Epigenetics, Department of Biomolecular Sciences, Faculty of Medicine, Saga University, Saga, Japan

[2]Department of Maternal–Fetal Biology, National Research Institute for Child Health and Development, Setagaya, Tokyo, Japan

[3]Department of Pediatrics, Kurume University, Kurume, Japan

[4]Department of Obstetrics and Gynecology, University of Toyama, Toyama, Japan

[5]Nishikyushu University, Kanzaki, Saga, Japan

Manuscript Received: 7 October 2011; Manuscript Accepted: 19 January 2012

Gain of methylation (GOM) at the H19-differentially methylated region (H19-DMR) is one of several causative alterations in Beckwith–Wiedemann syndrome (BWS), an imprinting-related disorder. In most patients with epigenetic changes at H19-DMR, the timing of and mechanism mediating GOM is unknown. To clarify this, we analyzed methylation at the imprinting control regions of somatic tissues and the placenta from two unrelated, naturally conceived patients with sporadic BWS. Maternal H19-DMR was abnormally and variably hypermethylated in both patients, indicating epigenetic mosaicism. Aberrant methylation levels were consistently lower in placenta than in blood and skin. Mosaic and discordant methylation strongly suggested that aberrant hypermethylation occurred after implantation, when genome-wide de novo methylation normally occurs. We expect aberrant de novo hypermethylation of H19-DMR happens to a greater extent in embryos than in placentas, as this is normally the case for de novo methylation. In addition, of 16 primary imprinted DMRs analyzed, only H19-DMR was aberrantly methylated, except for NNAT DMR in the placental chorangioma of Patient 2. To our knowledge, these are the first data suggesting when GOM of H19-DMR occurs. © 2012 Wiley Periodicals, Inc.

Key words: Beckwith–Wiedemann syndrome; H19-DMR; aberrant DNA methylation; after implantation

How to Cite this Article:
Higashimoto K, Nakabayashi K, Yatsuki H, Yoshinaga H, Jozaki K, Okada J, Watanabe Y, Aoki A, Shiozaki A, Saito S, Koide K, Mukai T, Hata K, Soejima H. 2012. Aberrant methylation of H19-DMR acquired after implantation was dissimilar in soma versus placenta of patients with Beckwith–Wiedemann syndrome.
Am J Med Genet Part A 158A:1670–1675.

INTRODUCTION

Beckwith–Wiedemann syndrome (BWS) is an imprinting-related condition characterized by macrosomia, macroglossia, and abdominal wall defects (OMIM #130650). The relevant imprinted chromosomal region in BWS, 11p15.5, consists of two independent imprinted domains, *IGF2/H19* and *CDKN1C/KCNQ1OT1*. Imprinted genes within each domain are regulated by two imprinting control regions (ICR), the H19-differentially methylated region (H19-DMR) or KvDMR1 [Weksberg et al., 2010]. Several causative alterations have been identified in patients with BWS: loss of methylation (LOM) at KvDMR1, gain of methylation (GOM) at H19-DMR, paternal uniparental disomy (UPD), *CDKN1C* mutations, and chromosomal abnormality involving 11p15 [Sasaki et al., 2007; Weksberg et al., 2010].

Additional supporting information may be found in the online version of this article.

Grant sponsor: Japan Society for the Promotion of Science; Grant number: 20590330; Grant sponsor: Ministry of Health, Labor, and Welfare; Grant sponsor: National Center for Child Health and Development.

*Correspondence to:
Hidenobu Soejima, M.D., Ph.D., Professor, Division of Molecular Genetics & Epigenetics, Department of Biomolecular Sciences, Faculty of Medicine, Saga University, 5-1-1 Nabeshima, Saga 849-8501, Japan.
E-mail: soejimah@med.saga-u.ac.jp

Article first published online in Wiley Online Library (wileyonlinelibrary.com): 10 May 2012
DOI 10.1002/ajmg.a.35335

© 2012 Wiley Periodicals, Inc.

Methylation of H19-DMR is erased in primordial germ cells (PGCs) but becomes reestablished during spermatogenesis [Li, 2002; Sasaki and Matsui, 2008]: this methylation regulates the expression of *IGF2* and *H19* by functioning as a chromatin insulator, restricting access to shared enhancers [Bell and Felsenfeld, 2000; Hark et al., 2000]. GOM on the maternal H19-DMR leads to expression of both *IGF2* alleles and silencing of both *H19* alleles. Dominant maternal transmissions of microdeletions and/or base substitutions within H19-DMR have recently been reported in a few patients of BWS with H19-DMR GOM [Demars et al., 2010]. However, when and how the GOM on the maternal H19-DMR occurs is not clear.

Here, we found epigenetic mosaicism in two BWS patients. We also found that GOM at H19-DMR was discordant in blood and skin versus placenta; specifically, methylation levels were lower in placental samples. These findings strongly suggest that aberrant methylation of H19-DMR occurred after implantation. As a result, we expect aberrant de novo methylation happens to a greater extent in embryos than in placentas.

MATERIALS AND METHODS

Patients

Two unrelated patients with sporadic BWS, Patient 1 (BWS047) and Patient 2 (bwsh21-015), were delivered by cesarean in the third trimester of pregnancy. The mothers of both patients conceived naturally. Patient 1 and Patient 2 met clinical criteria for BWS as described by Elliott et al. [1994] and Weksberg et al. [2001], respectively (Table I). The placenta of Patient 1 was large and weighed 1,065 g, but was without any pathological abnormality. The placenta of Patient 2 was also large, weighing 1,620 g, and had an encapsulated placental chorangioma, as reported previously [Aoki et al., 2011]. The standard G-banding chromosome analysis using peripheral blood samples showed no abnormalities in either patient. This study was approved by the Ethics Committee for Human Genome and Gene Analyses of the Faculty of Medicine, Saga University.

Southern Blot Analysis

Genomic DNA was extracted from embryo-derived somatic tissues and the placentas of the patients (Fig. 1). Methylation-sensitive Southern blots with *Bam*HI and *Not*I were employed for KvDMR1, and blots with *Pst*I and *Mlu*I were employed for H19-DMR, as described previously [Soejima et al., 2004]. Band intensity was measured using the FLA-7000 fluoro-image analyzer (Fujifilm, Tokyo, Japan). The methylation index (MI, %) was then calculated (Fig. 1). Southern blots with *Apa*I were used to identify the microdeletion of H19-DMR as described previously [Sparago et al., 2004].

Bisulfite Sequencing and Combined Bisulfite Restriction Analysis (COBRA)

Bisulfite sequencing covering the sixth CTCF binding site (CTS6) was performed. For COBRA, PCR products of each primary imprinted DMR were digested with the appropriate restriction endonucleases and were then separated using the MultiNA Microchip Electrophoresis System (Shimazdu, Japan). The methylation index was also calculated. All PCR primer sets used in this study have been listed in Supplementary Table SI (See Supporting Information online).

DNA Polymorphism Analyses

For quantitative polymorphism analyses, tetranucleotide repeat markers (*D11S1997* and *HUMTH01*) and a triplet repeat marker (*D11S2362*) from 11p15.4–p15.5 were amplified and separated by electrophoresis on an Applied Biosystems 3130 genetic analyzer (Applied Biosystems, NY); data were quantitatively analyzed with the GeneMapper software. The peak height ratios of paternal allele to maternal allele were calculated. A single nucleotide polymorphism (SNP) for the *Rsa*I recognition site in *H19* exon 5 (rs2839703) was also quantitatively analyzed using hot-stop PCR [Uejima et al., 2000]. Band intensity was measured using the FLA-7000 fluoro-image analyzer (Fujifilm).

Mutation Search of H19-DMR

To search for mutations in the binding sites of CTCF, OCT4, and SOX2, we sequenced a genomic region in and around H19-DMR, which included seven CTCF-binding sites, three OCT4 sites, and one SOX2 site.

TABLE I. Clinical Information of BWS Patients

Patient ID	Conception	Birth weight (gestational age)	Clinical features	Karyotype	Placental weight and pathology	Placental–fetal weight ratio
Patient 1 (BWS047)	Natural	4,506 g (36w2d)	macrosomia macroglossia abdominal wall defect hypoglycemia	46,XY	1,065 g no pathological findings	0.236
Patient 2 (bwsh21-015)	Natural	2,540 g (33w5d)	macrosomia macroglossia hypoglycemia renal malformation hepatosplenomegaly	46,XX	1,620 g placental chorangioma	0.638

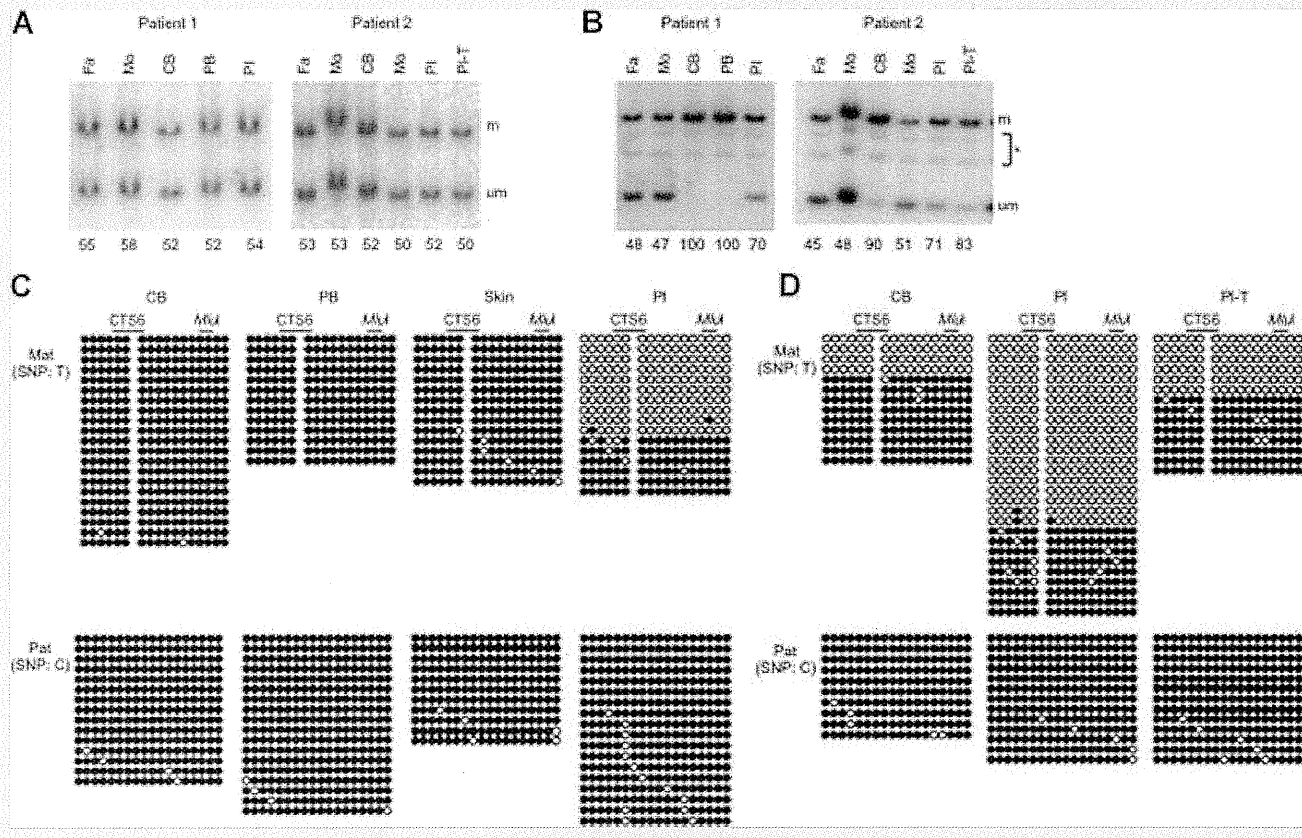

FIG. 1. Methylation analyses of KvDMR1 and H19-DMR. A: Methylation-sensitive Southern blots for KvDMR1. Genomic DNA was extracted from the cord blood, peripheral blood, skin, and placenta of Patient 1 and from the cord blood, placenta, and placental chorangioma of Patient 2. Methylation at KvDMR1 was normal in all samples analyzed. Methylation indices (MI, %) are shown under the figure. B: Methylation-sensitive Southern blots for H19-DMR. The MIs of blood samples were higher than the MIs of placental samples. MI was calculated using the equation $[M/(M+U)] \times 100$, where M is the intensity of the methylated band and U is the intensity of the unmethylated band. C: Bisulfite sequencing of H19-DMR in Patient 1. The two parental alleles were distinguishable by differences in SNPs. Both parental alleles were completely methylated in the cord blood, peripheral blood, and skin samples, and the maternal allele, which is normally unmethylated, was partially methylated in the placenta. D: Bisulfite sequencing of H19-DMR in Patient 2. Methylation of the maternal allele was higher in the cord blood than in the placenta or placental chorangioma. These results were consistent with the results of the Southern blot analysis. We confirmed complete methylation of paternal H19-DMR alleles and complete demethylation of maternal H19-DMR alleles in four normal control placentas that were heterozygous for identifiable SNPs (data not shown). Fa, father; Mo, mother; CB, cord blood; PB, peripheral blood; PI, placenta; PI-T, placental chorangioma; m, methylated band; um, unmethylated band; *, nonspecific bands; Mat, maternal allele; Pat, paternal allele; CTS6, sixth CTCF binding site; *MluI*, a restriction site approximately 80 bp downstream of CTS6 assayed by methylation-sensitive Southern blot and COBRA.

RESULTS

We first examined the methylation status of the two ICRs, KvDMR1, and H19-DMR, at 11p15.5 using methylation-sensitive Southern blot analysis. Methylation at KvDMR1 was normal in all samples collected (Fig. 1A); however, methylation at H19-DMR was aberrant (Fig. 1B). In Patient 1, hypermethylation at H19-DMR was complete in cord blood and peripheral blood samples (MI = 100%), and hypermethylation in the placenta was partial (MI = 70%). In Patient 2, H19-DMR was partially hypermethylated in cord blood (MI = 90%) but less so in the placenta and placental chorangioma (MI = 71% and MI = 83%, respectively). For further investigation of differences in methylation between the patients' somatic tissues and placentas, the CTS6 site was subjected to bisulfite sequencing (Fig. 1C and D). We could distinguish the two parental alleles in each patient sample using informative SNPs (rs10732516 and rs2071094). The maternal allele, which is normally unmethylated, was completely methylated in the cord blood, peripheral blood, and skin from Patient 1. However, in placental samples from Patient 1, the maternal allele was only partially methylated: 36% of all CpGs analyzed were methylated. Similar results were observed in Patient 2: the maternal allele in the cord blood was 68% methylated; however, the maternal allele was only 31% and 55% methylated in the placenta and chorangioma samples, respectively. The paternal alleles, which are normally fully methylated, were fully methylated in all samples. These findings supported the results of the Southern blots. Furthermore, we could not find any microdeletions or mutations in or around H19-DMR,

including seven CTCF-binding sites, three OCT4 sites, and one SOX2 site, indicating that there was no genetic cause of the hypermethylation (Fig. 2A and data not shown).

Next, we analyzed polymorphic markers at 11p15.4–p15.5 to determine whether copy number abnormalities or paternal UPD might be involved in these BWS patients. Although smaller PCR products were more easily amplified, paternal–maternal allele ratios in blood samples were between 0.92 and 1.33, indicating that both parental alleles were equally represented in both patients (Fig. 2B). Therefore, we could rule out copy number abnormality and paternal UPD within the patients' blood. We also investigated maternal contamination in the placenta. *D11S1997* and *HUMTH01* for Patient 1 and the *Rsa*I polymorphism in *H19* (rs2839703) for Patient 2 were used for this investigation because the mothers were expected to be homozygous for such polymorphisms. Thus, we investigated contamination of our samples by assessing the homozygosity of the polymorphisms in the mothers. The paternal–maternal ratios in Patient 1 were 0.94 and 1.03, indicating an equal contribution of both parental alleles and suggesting no contamination (Fig. 2B). In Patient 2, the ratios were 0.77 and 0.78 in the placenta and chorangioma, respectively, suggesting a small amount of contamination (Fig. 2C). However, such contamination was too

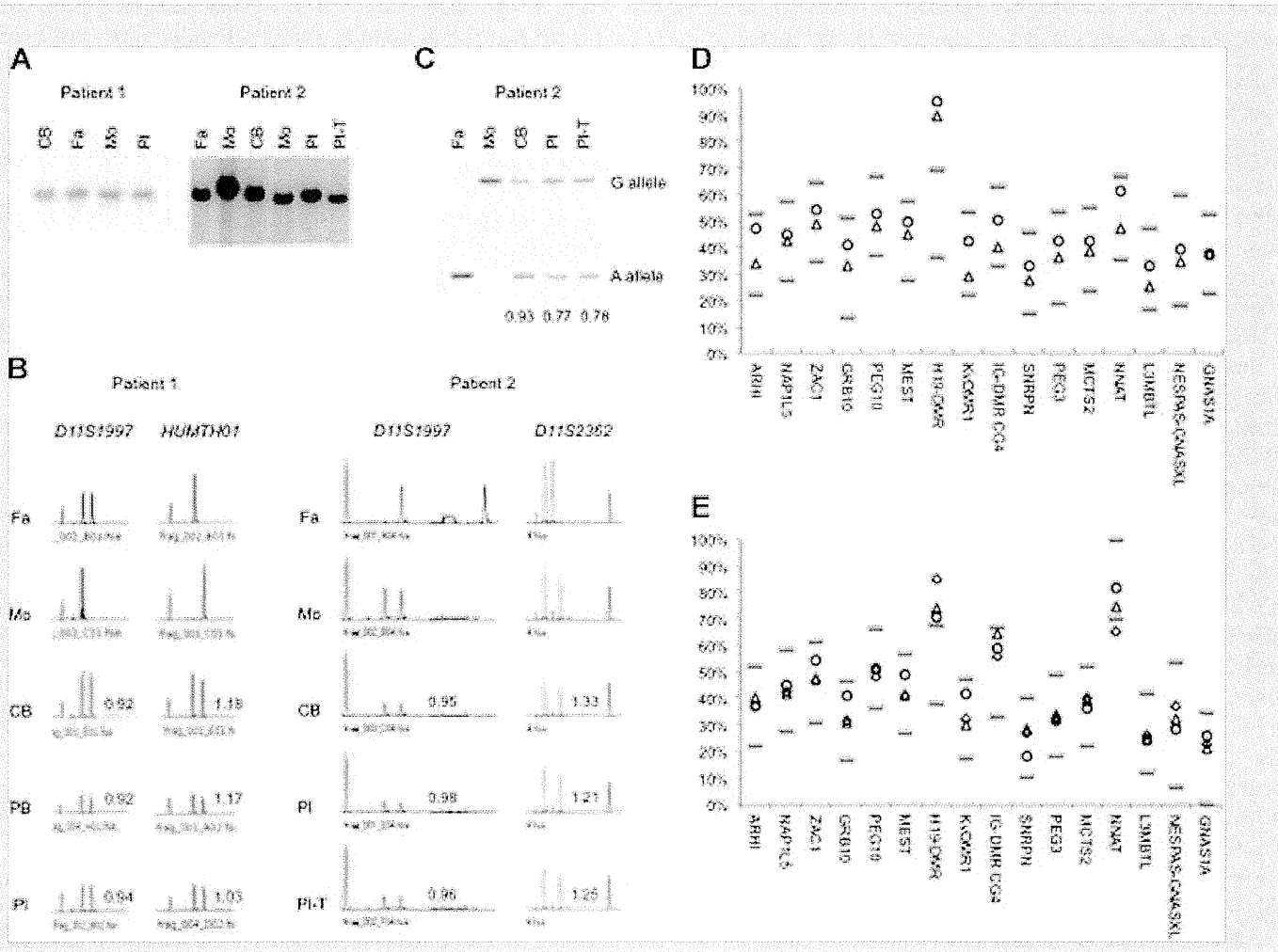

FIG. 2. Microdeletion analysis of H19-DMR, polymorphism analyses, and COBRA of primary imprinted DMRs in embryo-derived and placental samples. A: Southern blots identifying a microdeletion of H19-DMR. A genomic fragment (7.7 kb) generated by *Apa*I digestion, which included the entire H19-DMR, was evident in all samples, indicating that there was no microdeletion in this DMR. B: Microsatellite markers at 11p15.4–p15.5. The peak heights associated with each parental allele in all samples were quantitatively analyzed. The results indicated that both parental alleles were present and equally represented. C: Hot-stop PCR of an *Rsa*I polymorphic site in Patient 2. The ratios of paternal allele to maternal allele are shown under the figure. Although the ratios in the placenta and placental chorangioma are lower than in the cord blood, suggesting a small amount of maternal contamination, this was not enough to affect the results of the methylation analyses. COBRA of cord blood (D) and placentas (E), demonstrating that H19-DMR was hypermethylated. CTS6 is contained within H19-DMR. Methylation at other DMRs was normal in all samples, except for methylation at NNAT, which was aberrant in the placental chorangioma. Cord blood and placentas from 24 normal individuals were used as controls. The upper limit of normal methylation was defined as the higher of these two values: (1) the average of controls + 3 SD, or (2) the average + 15%. Similarly, the lower limit of normal methylation was definite as the lower of these two values: (1) the average of controls − 3 SD, or (2) the average − 15%. The upper and lower limits are indicated by gray bars. ○: Patient 1; △: Patient 2; ◇: placental chorangioma of Patient 2.

small to affect the results of the methylation analyses. In addition, sequence analysis did not show any mutations in *CDKN1C* (data not shown). These findings indicated that H19-DMR was aberrantly hypermethylated in both BWS patients and their associated placentas, but the aberrant methylation was consistently lower in the placenta, and that the H19-DMR GOM was strictly an isolated epimutation.

Finally, we analyzed the methylation status of 16 primary imprinted DMRs scattered throughout the genome-using COBRA (Fig. 2D and E). Only H19-DMR showed aberrant methylation among all primary DMRs in all samples, except for NNAT DMR, which was abnormal only in the placental chorangioma, indicating that the *IGF2/H19* imprinted domain was targeted for aberrant methylation in both somatic tissues and the placenta.

DISCUSSION

Methylation associated with parental imprints are erased in PGC and reestablished during gametogenesis in a sex-specific manner. The paternal pronucleus in the zygote undergoes active demethylation; extensive passive demethylation then ensues on maternal and paternal chromosomes during the pre-implantation period. After implantation, de novo methylation results in a rapid increase in DNA methylation in the inner cell mass (ICM), which gives rise to the entire embryo; in contrast, de novo methylation is either inhibited or not maintained in the trophoblast, which gives rise to the placenta [Li, 2002; Sasaki and Matsui, 2008]. The imprinted DMRs, however, escape these demethylation and de novo methylation events that occur in early embryogenesis. H19-DMR GOM in BWS patients is considered an error in imprint erasure in female PGCs [Horsthemke, 2010]. However, H19-DMR GOM, whether with or without microdeletions within H19-DMR, was partial, indicating a mosaic of normal cells and aberrantly methylated cells [Sparago et al., 2007; Cerrato et al., 2008]. These findings demonstrated that aberrant hypermethylation at H19-DMR was acquired after fertilization, although the precise timing was unknown.

Both participants in this study had isolated GOM at H19-DMR. The partial and variable hypermethylation among samples suggested epigenetic mosaicism. Furthermore, methylation levels in the placentas were lower than those in the blood and skin, suggesting that the aberrant methylation was acquired after implantation—when genome-wide de novo methylation normally occurs. Aberrant de novo methylation at H19-DMR is expected to be more widespread in the embryo than in the placenta, as this is normally the case for de novo methylation [Li, 2002; Sasaki and Matsui, 2008]; this disparity in efficiency could lead to the discordance between hypermethylation in trophoblast-derived placenta and that in embryo-derived blood and skin. This hypothesis is supported by a mouse experiment in which a mutant maternal allele harboring a deletion of four CTCF binding sites was hypomethylated in oocytes and blastocysts, yet was highly methylated after implantation [Engel et al., 2006]. To our knowledge, this is the first evidence demonstrating that aberrant hypermethylation of maternal H19-DMR is acquired after implantation in humans.

We found that of 16 primary imprinted DMRs analyzed, only H19-DMR showed aberrant methylation; even methylation at IG-DMR CG4, another paternally methylated, primary imprinted DMR, was normal in our patients. Although we only studied two patients, this finding indicated that the *IGF2/H19* imprinted domain in both the embryo and placenta was more susceptible than other imprinted domains to aberrant methylation acquired after implantation.

In conclusion, we found that methylation of H19-DMR was discordant in embryo-derived somatic tissue and placenta, strongly suggesting that the aberrant de novo methylation occurred after implantation. However, the precise mechanism of isolated H19-DMR GOM is still unknown. Since no mutations in *CTCF*, an important trans-acting imprinting factor, were found in these patients with isolated GOM at H19-DMR, the potential for mutations in the OCT and SOX transcription factors should be investigated because mutations of OCT-binding sites have previously been found in a few patients with H19-DMR GOM [Cerrato et al., 2008; Demars et al., 2010].

ACKNOWLEDGMENTS

This study was supported, in part, by a Grant-in-Aid for Scientific Research (C) (No. 20590330) from the Japan Society for the Promotion of Science, a Grant for Research on Intractable Diseases from the Ministry of Health, Labor, and Welfare, and a Grant for Child Health and Development from the National Center for Child Health and Development.

REFERENCES

Aoki A, Shiozaki A, Sameshima A, Higashimoto K, Soejima H, Saito S. 2011. Beckwith–Wiedemann syndrome with placental chorangioma due to H19-differentially methylated region hypermethylation: A case report. J Obstet Gynaecol Res 37:1872–1876.

Bell AC, Felsenfeld G. 2000. Methylation of a CTCF-dependent boundary controls imprinted expression of the Igf2 gene. Nature 405:482–485.

Cerrato F, Sparago A, Verde G, De Crescenzo A, Citro V, Cubellis MV, Rinaldi MM, Boccuto L, Neri G, Magnani C, D'Angelo P, Collini P, Perotti D, Sebastio G, Maher ER, Riccio A. 2008. Different mechanisms cause imprinting defects at the IGF2/H19 locus in Beckwith–Wiedemann syndrome and Wilms' tumour. Hum Mol Genet 17:1427–1435.

Demars J, Shmela ME, Rossignol S, Okabe J, Netchine I, Azzi S, Cabrol S, Le Caignec C, David A, Le Bouc Y, El-Osta A, Gicquel C. 2010. Analysis of the IGF2/H19 imprinting control region uncovers new genetic defects, including mutations of OCT-binding sequences, in patients with 11p15 fetal growth disorders. Hum Mol Genet 19:803–814.

Elliott M, Bayly R, Cole T, Temple IK, Maher ER. 1994. Clinical features and natural history of Beckwith–Wiedemann syndrome: Presentation of 74 new cases. Clin Genet 46:168–174.

Engel N, Thorvaldsen JL, Bartolomei MS. 2006. CTCF binding sites promote transcription initiation and prevent DNA methylation on the maternal allele at the imprinted H19/Igf2 locus. Hum Mol Genet 15:2945–2954.

Hark AT, Schoenherr CJ, Katz DJ, Ingram RS, Levorse JM, Tilghman SM. 2000. CTCF mediates methylation-sensitive enhancer-blocking activity at the H19/Igf2 locus. Nature 405:486–489.

Horsthemke B. 2010. Mechanisms of imprint dysregulation. Am J Med Genet C Semin Med Genet 154C:321–328.

Li E. 2002. Chromatin modification and epigenetic reprogramming in mammalian development. Nat Rev Genet 3:662–673.

Sasaki H, Matsui Y. 2008. Epigenetic events in mammalian germ-cell development: Reprogramming and beyond. Nat Rev Genet 9:129–140.

Sasaki K, Soejima H, Higashimoto K, Yatsuki H, Ohashi H, Yakabe S, Joh K, Niikawa N, Mukai T. 2007. Japanese and North American/European patients with Beckwith–Wiedemann syndrome have different frequencies of some epigenetic and genetic alterations. Eur J Hum Genet 15: 1205–1210.

Soejima H, Nakagawachi T, Zhao W, Higashimoto K, Urano T, Matsukura S, Kitajima Y, Takeuchi M, Nakayama M, Oshimura M, Miyazaki K, Joh K, Mukai T. 2004. Silencing of imprinted CDKN1C gene expression is associated with loss of CpG and histone H3 lysine 9 methylation at DMR-LIT1 in esophageal cancer. Oncogene 23:4380–4388.

Sparago A, Cerrato F, Vernucci M, Ferrero GB, Silengo MC, Riccio A. 2004. Microdeletions in the human H19 DMR result in loss of IGF2 imprinting and Beckwith–Wiedemann syndrome. Nat Genet 36:958–960.

Sparago A, Russo S, Cerrato F, Ferraiuolo S, Castorina P, Selicorni A, Schwienbacher C, Negrini M, Ferrero GB, Silengo MC, Anichini C, Larizza L, Riccio A. 2007. Mechanisms causing imprinting defects in familial Beckwith–Wiedemann syndrome with Wilms' tumour. Hum Mol Genet 16:254–264.

Uejima H, Lee MP, Cui H, Feinberg AP. 2000. Hot-stop PCR: A simple and general assay for linear quantitation of allele ratios. Nat Genet 25: 375–376.

Weksberg R, Nishikawa J, Caluseriu O, Fei YL, Shuman C, Wei C, Steele L, Cameron J, Smith A, Ambus I, Li M, Ray PN, Sadowski P, Squire J. 2001. Tumor development in the Beckwith–Wiedemann syndrome is associated with a variety of constitutional molecular 11p15 alterations including imprinting defects of KCNQ1OT1. Hum Mol Genet 10:2989–3000.

Weksberg R, Shuman C, Beckwith JB. 2010. Beckwith–Wiedemann syndrome. Eur J Hum Genet 18:8–14.

FEBS Letters 586 (2012) 827–833

journal homepage: www.FEBSLetters.org

Imprinted DNA methylation reprogramming during early mouse embryogenesis at the *Gpr1-Zdbf2* locus is linked to long *cis*-intergenic transcription

Hisato Kobayashi [a], Takayuki Sakurai [a], Shun Sato [b,1], Kazuhiko Nakabayashi [b], Kenichiro Hata [b], Tomohiro Kono [a,c,*]

[a] *Department of BioScience, Tokyo University of Agriculture, 1-1-1 Sakuragaoka, Setagaya-ku, Tokyo 156-8502, Japan*
[b] *Department of Maternal-Fetal Biology, National Research Institute for Child Health and Development, 2-10-1 Okura, Setagaya-ku, Tokyo 157-8535, Japan*
[c] *Genome Research Center, NODAI Research Institute, Tokyo University of Agriculture, 1-1-1 Sakuragaoka, Setagaya-ku, Tokyo 156-8502, Japan*

ARTICLE INFO

Article history:
Received 12 January 2012
Revised 27 January 2012
Accepted 31 January 2012
Available online 9 February 2012

Edited by Ned Mantei

Keywords:
DNA methylation
Genomic imprinting
Imprinting control region
Differentially methylated region
Non-coding RNA

ABSTRACT

The paternally-expressed imprinted genes *Gpr1* and *Zdbf2* form a gene cluster wherein the imprinted-methylated regions of these two genes differ. We identified a novel, paternally expressed, long intergenic non-coding *Zdbf2* variant (*Zdbf2linc*) transcribed from maternally methylated *Gpr1* DMR during early embryogenesis in the mouse. While the *Gpr1* DMR displayed biallelic hypermethylation, *Zdbf2linc* expression was rarely observed in the post-gastrulation, despite a positive correlation between the methylation of *Zdbf2* DMRs and the mono-allelic transcription of the original *Zdbf2* coding variant. Furthermore, lack of the maternal methylation imprint resulted in the biallelic expression of both coding and non-coding *Zdbf2* transcripts as well as complete methylation of *Zdbf2* DMRs. Globally, our findings suggest the role of *Zdbf2linc* in the establishment of secondary epigenetic modifications after implantation.
© 2012 Federation of European Biochemical Societies. Published by Elsevier B.V. All rights reserved.

1. Introduction

Functional non-equivalence between parental genomes in mammals is caused by parental origin-specific mono-allelic expression of certain genes, termed "imprinted" genes [1]. To date, over one hundred imprinted genes have been identified in humans and mice (MRC Mammalian Genetics Unit, Harwell, UK, http://www.har.mrc.ac.uk/research/genomic_imprinting), most of which form clusters in specific genomic regions responsible for the abnormal phenotypes of uniparental disomies. Imprinted gene clusters are marked epigenetically and imprinted differentially in the parental germline, depending on the parent. Differentially methylated regions (DMRs), which exhibit parent-of-origin-dependent DNA methylation patterns, have been identified within or near imprinted genes. Two classes of DMRs have been identified: germline DMRs (primary DMRs), which acquire methylation during gametogenesis, and somatic DMRs (secondary DMRs), which establish their allelic methylation patterns after fertilization, most likely through the influence of the germline DMRs at each gene cluster [2–6]. Gene knockout experiments in mice point to the involvement of DNA methylation in this process. De novo methyltransferase *Dnmt3a* and de novo methyltransferase-related protein *Dnmt3L* are required for the establishment of primary methylation imprints in paternal and maternal germlines, as well as the mono-allelic expression patterns of imprinted genes in the embryo proper [7–9]. The targeted deletion of some germline DMRs in mice has also been found to result in the aberrant expression of single or several associated imprinted genes, as well as the loss of the allelic methylation of secondary DMRs [10–19]. Such germline DMRs are called imprinting control regions (ICRs), and act as long-range *cis*-acting regulatory elements.

An imprinted gene cluster containing the *Gpr1* (G protein-coupled receptor 1) and *Zdbf2* (zinc finger, DBF-type containing 2) genes has been identified in mouse chromosome 1; both are specifically expressed from the paternal allele [20–22]. *Zdbf2* was found to have imprinted expression in various embryonic and adult tissues, whereas *Gpr1* showed kidney-specific imprinted expression (Fig. 1A). However, functional roles of these genes in biological processes remain undetermined. Multiple methylome analyses have identified two kinds of imprinted methylated regions in this cluster: maternal allele-specific methylation at a CpG island in *Gpr1* intron 2 (*Gpr1* DMR), and paternal allele-specific

* Corresponding author at: Department of BioScience, Tokyo University of Agriculture, 1-1-1 Sakuragaoka, Setagaya-ku, Tokyo 156-8502, Japan. Fax: +81 354772543.
E-mail address: tomohiro@nodai.ac.jp (T. Kono).
[1] Current address: Department of Obstetrics and Gynecology, Yamaguchi University Graduate School of Medicine, Minamikogushi 1-1-1, Ube, Yamaguchi 755-8505, Japan.

0014-5793/$36.00 © 2012 Federation of European Biochemical Societies. Published by Elsevier B.V. All rights reserved.
doi:10.1016/j.febslet.2012.01.059

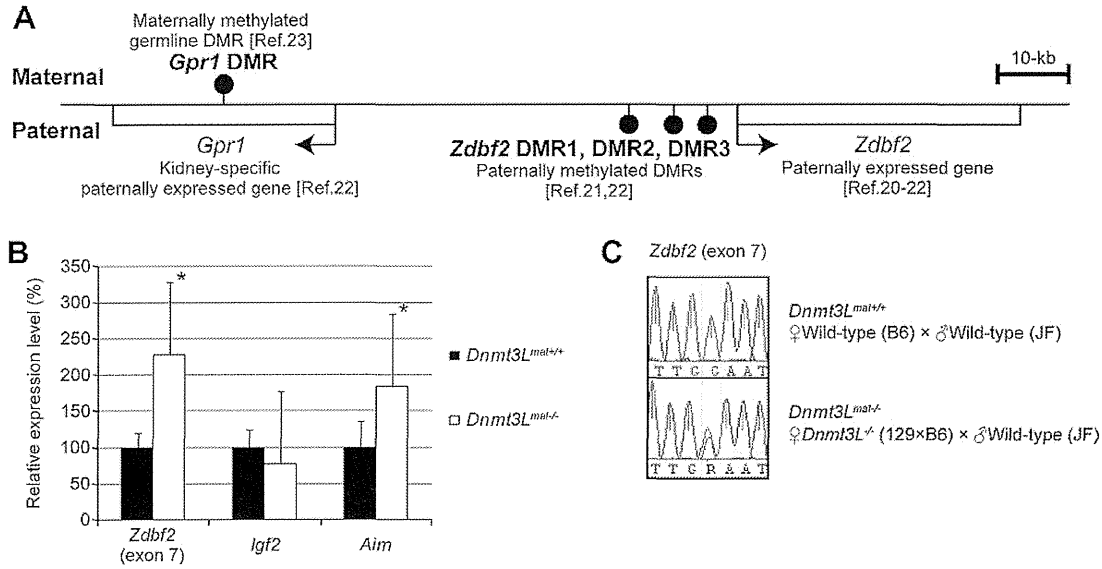

Fig. 1. Comparison of *Zdbf2* gene expression in wild-type and $Dnmt3L^{mat-/-}$ embryos. (A) Schematic representation of the imprinted *Gpr1-Zdbf2* domain on mouse chromosome 1C2. Open boxes represent the locations of the two paternally expressed genes; arrows denote the transcriptional direction of these genes. The positions of the differentially methylated regions (DMRs) are indicated by filled pins on the methylated alleles. (B) Quantitative real-time RT-PCR expression analysis of paternally expressed genes *Zdbf2* (exon 7), *Igf2*, and *Aim* in E9.5 mouse embryos from $Dnmt3L^{mat+/+}$ and $Dnmt3L^{mat-/-}$ mice ($n \geqslant 3$). Expression levels of each gene were normalized to those of the housekeeping gene *Gapdh*. Error bars represent SEM ($n = 3$), while asterisks indicate $P < 0.01$ (Student's *t*-test). *Igf2* and *Aim* are regulated by paternal (*H19* DMR) and maternal (*Igf2r* DMR2) methylation imprints, respectively. (C) Allelic expression analysis of *Zdbf2* was performed using F_1 hybrid crosses between wild-type C57BL/6 (B6) or *Dnmt3L*-deficient 129SvJae × C57BL/6N (129 × B6) females and JF1/Msf (JF) males. Maternal and paternal alleles were distinguished by an SNP (A/G at chr1. 63,361,080; highlighted in yellow).

methylation at the intergenic regions between the *Gpr1* and *Zdbf2* genes (*Zdbf2* DMR1, DMR2, and DMR3) [21–23]. However, the identity of the DMR that acts as a true ICR on the *Gpr1-Zdbf2* locus remains unknown.

Similar to the *Gpr1-Zdbf2* gene cluster, three other imprinted gene clusters, *Gnas-Nespas*, *Kcnq1ot1*, and *Igf2r-Airn*, have been found to have contradicting imprinted methylation. In these clusters, maternal allele-specific methylations act as ICRs, while the long non-coding RNAs transcribed from them have a role in silencing genes in *cis* through gene- and lineage-specific repressive chromatin modifications [24–26]. Other DMRs may additionally become methylated on the paternal allele after fertilization as somatic DMRs. Furthermore, recent studies have shown that transcription through *Gnas* DMRs is required for their allele-specific methylation to be established during pre- or post-fertilization [26,27]. It is important to elucidate the relationship between imprinted methylation and gene expression profiles on a gene cluster in order to understand the mechanisms by which imprinted expression is regulated.

In this study, we identified a novel, long (>100 kb), imprinted non-coding *Zdbf2* variant transcribed from the *Gpr1* DMR in mice, which showed paternal-allele-specific expression in early embryonic cells. Its expression was found to be associated with the methylation of the *Gpr1* DMR in *cis*. Our results indicate that maternal-allele-specific methylation of the *Gpr1* DMR may directly regulate the imprinted expression of this long non-coding RNA. The transcription of the *Zdbf2* variant may be essential for the establishment of the somatic intergenic differential methylation of *Zdbf2* DMRs that regulates imprinted *Zdbf2* expression after implantation.

2. Materials and methods

2.1. Sample preparation

Mouse early embryos, embryonic stem (ES) cells, and adult tissues were prepared as described previously [6,21,28]. To use DNA polymorphisms for allele discrimination, wild-type reciprocal F_1 hybrids ($Dnmt3L^{mat+/+}$) were obtained by crossing C57BL/6 (B6; Clea Japan, Tokyo, Japan) and JF1/Msf (JF) mice. $Dnmt3L^{mat-/-}$ embryos were obtained by crossing *Dnmt3L*-deficient female (129SvJae × B6 hybrid genetic background) and wild-type JF mice. ES cells were derived from B6 mice (Clea Japan).

2.2. Real-time RT-PCR and allelic expression analyses

Total RNA from E3.5 blastocysts, E5.5 whole embryos, E6.5, E7.5 embryonic tissues (extra-embryonic tissues were removed), and E9.5 whole embryos (yolk sacs and amnions were removed) [6], and ES cells was isolated using the Allprep DNA/RNA micro kit (Qiagen, Valencia, CA) and TRIzol reagent (Invitrogen, Carlsbad, CA). Genomic DNA-free total RNA was reverse transcribed to cDNA with SuperScript III (Invitrogen). Quantitative analysis for *Igf2*, *Airn*, and *Zdbf2* gene expression was performed in a 7500 Real-time PCR system (Applied Biosystems, Foster City, CA) with SYBR Green PCR Master Mix (Applied Biosystems). Relative expression levels of each gene were normalized to those of the *Gapdh* or *Actb* housekeeping genes. RT-PCR and direct sequencing for *Zdbf2* variants were performed using an ABI PRISM 3730xl genetic analyzer (Applied Biosystems), as described earlier [21]. Primer sequences and PCR conditions are listed in Table 1.

2.3. Rapid amplification of cDNA ends analysis

The 5′-region of the mouse *Zdbf2* gene was obtained using the GeneRacer Kit (Invitrogen). Total RNA was prepared from ES cells, and two rounds of PCR were carried out using TaKaRa EX Taq (TaKaRa) under the following conditions: 25 cycles of 30 s at 94 °C, 30 s at 64 °C, 1 min at 72 °C for the first PCR; and 20 cycles of 30 s at 94 °C, 30 s at 60 °C, and 1 min at 72 °C for the second PCR. The *Zdbf2* gene-specific primer sets used for the nested PCR were as follows: anti-sense 5RA8: 5′-AGCTGAGGACCCGGAATCCT CACAT-3′ for the first PCR and anti-sense 5RA9: 5′-TGAGGACCCGG AATCCTCACATGGT-3′ for the second PCR. The amplified products were sequenced directly, after purification.

Table 1
PCR primer information.

Zdbf2 exon A&B	chr1: 63,247,197–63,247,248 63,254,089–63,254,143	5′-TTGAACTTGGCTTACCAGTGTGT-3′ 5′-TTTCTCAAGGTGAAACAGGGAGT-3′	107	RT, Real-time	94 °C, 1 min	94 °C, 30 s	60 °C, 30 s	72 °C, 30 s	72 °C, 5 min	40	
Zdbf2 exon 5	chr1: 63,337,249–63,337,356	5′-CAGACCCTCACTAAAGGAAAAACT-3′ 5′-CTGTCCATTGTTCTTCATTACTTC-3′	106	RT, Real-time	94 °C, 1 min	94 °C, 30 s	60 °C, 30 s	72 °C, 30 s	72 °C, 5 min	40	
Zdbf2 exon 7	chr1: 63,360,906–63,361,130	5′-TGATCCACAGTTATGGACTT-3′ 5′-TCAAACTGACATCACATGG-3′	225	Real-time	95 °C, 10 min	95 °C, 15 s	60 °C, 1 min			40	[21]
Igf2	chr7: 149,839,164–149,839,745	5′-GGAGATGTCCAGCAACCATC-3′ 5′-CTGAAGCAATGACATGCCAC-3′	582	Real-time	95 °C, 10 min	95 °C, 15 s	60 °C, 1 min			40	
Airn	chr17: 12,935,735–12,935,961	5′-GTGGATTCAGGTTTCATG-3′ 5′-GGCCCAGATATAGAATGT-3′	227	Real-time	95 °C, 10 min	95 °C, 15 s	60 °C, 1 min			40	
Gapdh	chr6: 125,112,864–125,113,058 125,113,157–125,113,201	5′-GTCGTGGAGTCTACTGGTGTC-3′ 5′-GAGCCCTTCCACAATGCCAAA-3′	244	Real-time	94 °C, 1 min	94 °C, 30 s	57 °C, 30 s	72 °C, 30 s	72 °C, 5 min	40	
Actb	chr5:143,664,856–143,665,043	5′-AGGTGACAGCATTGCTTCTG-3′ 5′-GCTGCCTCAACACCTCAAC-3′	188	RT, Real-time	95 °C, 10 min	95 °C, 15 s	60 °C, 1 min			40	
Gpr1 DMR	chr1: 63,246,988–63,247,117	5′-AGATTACGTTAGTTTGGAATT-3′ 5′-AACACTAATCACCAAATAATTC-3′	130	Bisulfite	94 °C, 1 min	94 °C, 30 s	57 °C, 30 s	72 °C, 30 s	72 °C, 5 min	40	[23]
Zdbf2 DMR1	chr1: 63,306,143–63,306,507	5′-TGTGTATAGGTTTGTATGGTTTGTT-3′ 5′-ATAATCAACTACYAAAAAAACCCTAA-3′	365	Bisulfite	94 °C, 1 min	94 °C, 30 s	57 °C, 30 s	72 °C, 30 s	72 °C, 5 min	40	[22]
Zdbf2 DMR2	chr1: 63,311,117–63,311,450	5′-TAAATAAATATAAAGGGTTGGTTAGTT-3′ 5′-AAATCAAACTACAAACTCCAAACTA-3′	334	Bisulfite	94 °C, 1 min	94 °C, 30 s	60 °C, 30 s	72 °C, 30 s	72 °C, 5 min	40	[22]
Zdbf2 DMR3	chr1: 63,314,651–63,314,991	5′-ATTAACATATTTAGATTATGGATAGAT-3′ 5′-AAAATAAACTCTCCAAAACCAAAAA-3′	341	Bisulfite	94 °C, 1 min	94 °C, 30 s	60 °C, 30 s	72 °C, 30 s	72 °C, 5 min	40	[21]

2.4. Bisulfite sequencing analysis

Genomic DNA samples were isolated from *Dnmt3L*$^{mat+/+}$ (F_1 hybrid of B6 and JF) and *Dnmt3L*$^{mat-/-}$ embryos at the E3.5–E9.5 stages, as well as from the kidneys and hearts of 9-week-old female *Dnmt3L*$^{mat+/+}$ mice. Genomic DNA was treated with sodium bisulfite using the EpiTect Bisulfite Kit (Qiagen). The bisulfite-treated DNA was amplified by PCR with TaKaRa Taq Hot Start Version (TaKaRa) for *Gpr1* and *Zdbf2* DMRs. The primers and PCR conditions for the amplification are listed in Table 1. Subcloning and sequencing analyses were performed as described in a previous study [21]. Visualization and quantification of bisulfite sequence data for CpG methylation was performed using the QUMA web-based tool [29].

3. Results

3.1. Allelic expression analysis of Zdbf2 in mouse embryos lacking maternal methylation imprints at the post-gastrula stage

To determine if *Zdbf2* is regulated by maternal or paternal methylation imprints, we investigated *Zdbf2* expression patterns using real-time PCR and allelic expression analyses in mouse embryos at the E9.5 post-gastrula stage. The fetuses derived from wild-type and *Dnmt3L*-deficient female (*Dnmt3L*$^{mat-/-}$) mice, which lack maternal methylation imprints, were examined. Interestingly, an analysis of the 3′-UTR at exon 7 of the *Zdbf2* transcript showed biallelic expression and approximately twofold increased expression in *Dnmt3L*$^{mat-/-}$ embryos when compared with wild-type embryos, which showed paternal-allele specific expression (Fig. 1B and C). This concurs with what has been observed to occur with the *Airn* gene (Fig. 1B), which is paternally expressed under the control of the maternal methylation imprint (*Igf2r* DMR2), suggesting that *Zdbf2* expression is regulated by a *Dnmt3L*-mediated maternal methylation imprint, whereby the maternally methylated *Gpr1* DMR may act as an ICR for this imprinted locus. However, bisulfite sequencing analysis surprisingly showed that the *Gpr1* DMR was biallelically hypermethylated in E9.5 embryos (Fig. 2A), whereas its maternal-allele-specific methylation was maintained until at least the blastocyst stage [23].

3.2. Loss of differential methylation at Gpr1 DMR during embryonic development

To reveal the timing and progression of differential methylation changes over the course of embryonic development, the allelic methylation pattern of the *Gpr1* DMR was examined between the blastula and gastrula stages in mouse embryos at E3.5 (blastocyst), E5.5, E6.5, E7.5 (early- to late-gastrulation), and E9.5 (post-gastrulation). Although complete maternal-allele-specific methylation (*i.e.*, paternal-allele-specific hypomethylation) at the *Gpr1* DMR was maintained during the E3.5–E5.5 stages, the methylation of the paternal allele was significantly increased at subsequent stages (Fig. 2B). Hence, both maternal and paternal alleles were almost completely methylated at the E9.5 stage in wild-type (and even *Dnmt3L*$^{mat-/-}$) embryos (Fig. 2A). Adult somatic tissues, including the kidney, also showed biallelic hypermethylation of the *Gpr1* DMR (Fig. 2A), demonstrating that the kidney-specific imprinted expression of *Gpr1* is not associated with *Gpr1* DMR methylation. These results show that *Gpr1* DMR gains biallelic methylation after implantation, and that the methylation status of this DMR is not associated with the imprinted expression of *Zdbf2* or *Gpr1*, at least after gastrulation.

3.3. Allelic expression analysis of Zdbf2linc

Whereas our results showed that imprinted *Zdbf2* expression was controlled by maternal methylation imprint, maternally meth-

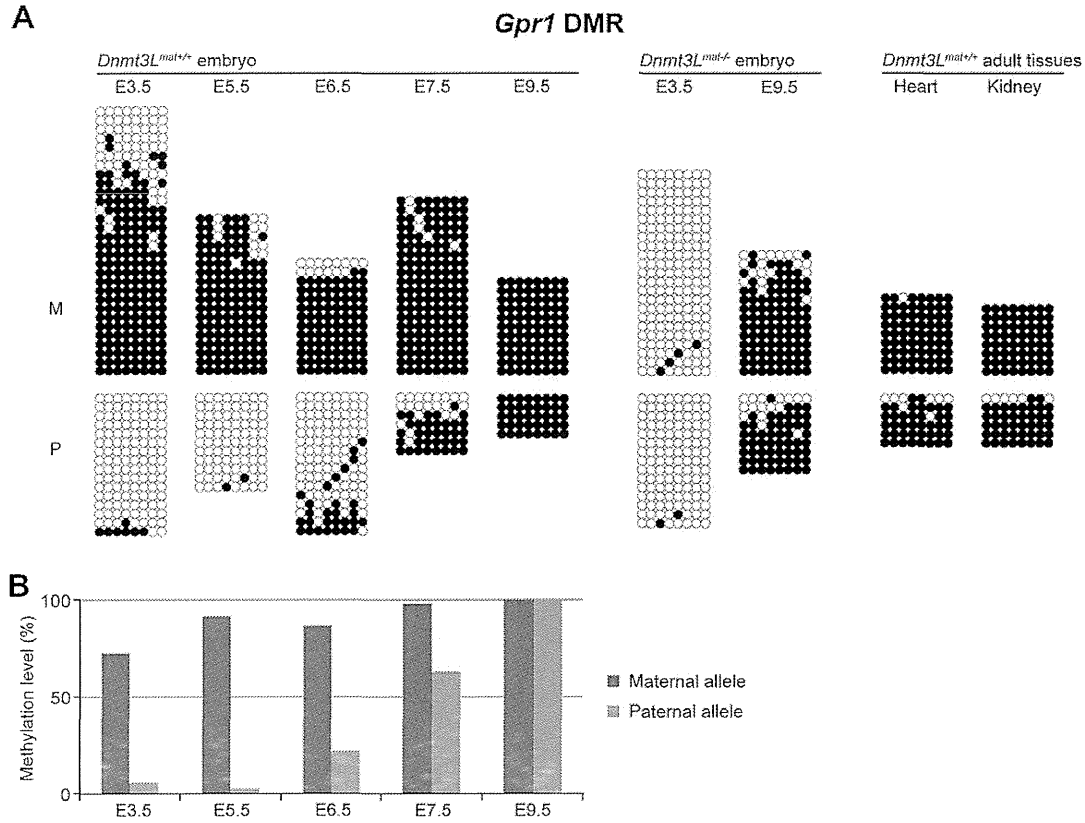

Fig. 2. DNA methylation profile of the *Gpr1* DMR. (A) Bisulfite sequencing analysis of the *Gpr1* DMR in wild-type and *Dnmt3L*$^{mat-/-}$ mouse embryos and adult tissues. Each row of circles represents the results of an independent sequencing reaction. The open and closed circles denote unmethylated and methylated CpGs, respectively. M and P indicate the maternally inherited B6 or 129 × B6 alleles and the paternally inherited JF allele, respectively. Both alleles were discriminated by three polymorphisms [23]. (B) Differential methylation status between M and P alleles during embryogenesis. CpG methylation levels of maternal and paternal alleles are represented by red and blue bars, respectively. These histograms were obtained from bisulfite sequencing analyses shown in (A).

ylated *Gpr1* DMR lost its mono-allelic methylation during gastrulation. To explain the apparent contradiction of the *Gpr1* DMR methylation status being unassociated with the imprinted expression of either the *Zdbf2* or *Gpr1* genes, we focused on a long intergenic non-coding RNA (lincRNA) located within the *Gpr1-Zdbf2* locus (Fig. 3A). This 114-kb lincRNA, which we named *Zdbf2linc*, had previously been identified in mouse ES cells by massively parallel cDNA sequencing (RNA-seq) and chromatin immunoprecipitation sequencing (ChIP-seq) [30]. *Zdbf2linc* is a splice variant of *Zdbf2* that contains seven exons, including three unique exons within intron 2 of the *Gpr1* gene (exon A and B), the *Gpr1/Zdbf2* intergenic region (exon C), and exons 3, 4, 6, and 7 of the *Zdbf2* gene (according to NCBI RefSeq). A long-range splice form of *Zdbf2linc* lacking exon C was also identified in ES cells by 5′ rapid amplification of cDNA ends (RACE) (Fig. 3A). Interestingly, the transcription start site of *Zdbf2linc* overlaps the *Gpr1* DMR. To determine if *Zdbf2linc* is detectable in vivo and is imprinted, we performed RT-PCR and allelic expression analysis in early to mid-term mouse embryos. *Zdbf2linc* expression was detected from E3.5 to E7.5 (Fig. 3B and C), during which time paternal-allele-specific expression was observed (Fig. 3D). Quantitative RT-PCR showed higher expression of *Zdbf2linc* than that of the original *Zdbf2* coding variant (including exon 5) in blastocysts and ES cells (Fig. 3C). Although *Zdbf2linc* was undetectable at E9.5, the expression of the original *Zdbf2* variant was clearly detected (Fig. 3B). Interestingly, the timing of *Zdbf2linc* repression was nearly identical to that of the loss of the differential methylation of the *Gpr1* DMR. Furthermore, *Dnmt3L*$^{mat-/-}$ embryos showed biallelic expression of *Zdbf2linc*. These findings indicate that methylation at *Gpr1* DMR may directly repress *Zdbf2linc* expression in *cis*.

3.4. Erasure and re-establishment of paternal-allele-specific methylation at Zdbf2 DMRs

While the methylation of *Gpr1* DMR and *Zdbf2linc* expression were correlated in *cis*, the epigenetic regulation of the original *Zdbf2* variant, which is expressed exclusively from the paternal allele after the E9.5 stage (Fig. 3B), remains unclear. We therefore investigated the methylation patterns of the *Zdbf2* DMRs present in the intragenic region of *Zdbf2linc*. All DMRs showed male-germ-cell specific hypermethylation in previous studies [21–23] and paternal-allele-specific hypermethylation in E9.5 embryos in this study (Fig. 4 middle); however, our previous DNA methylome analyses have shown that *Zdbf2* DMRs are deeply undermethylated in blastocysts [23]. Allelic methylation analyses performed in this study further confirmed that both the paternal and maternal alleles are unmethylated at the *Zdbf2* DMR3 in blastocysts (Fig. 4 left). Taken together, our results demonstrate that paternal-allele-specific methylation of the *Zdbf2* DMRs established in germ cells are erased after fertilization and re-established after implantation. Interestingly, biallelic hypermethylation of the *Zdbf2* DMRs was observed in *Dnmt3L*$^{mat-/-}$ embryos at E9.5 (Fig. 4 right), which is similar to the methylation pattern observed for the somatic DMR (*Nesp* DMR) in the imprinted *Gnas* cluster [17]. This suggests that not only are the *Zdbf2* DMRs in the intragenic region of *Zdbf2linc* somatic (secondary), but that the methylation of *Zdbf2* DMRs is

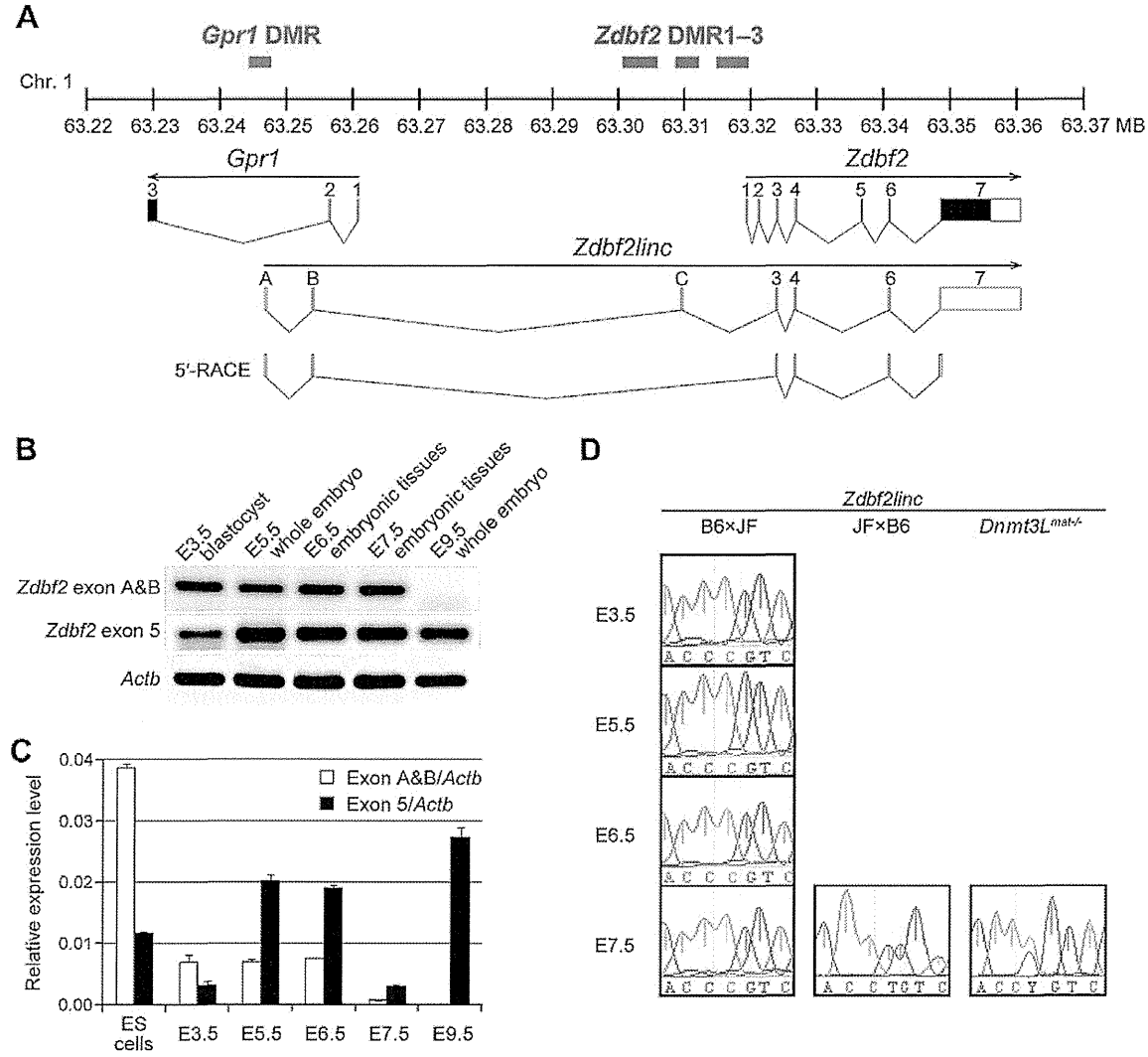

Fig. 3. Quantitative and allelic-specific expression analyses of *Zdbf2linc*. (A) Schematic physical map of the imprinted *Gpr1-Zdbf2* domain showing three paternally expressed transcripts and the 5′-RACE sequence. Red and blue bars represent maternally or paternally methylated DMRs, respectively. (B) Expression of two variants of *Zdbf2* during embryonic development. Forty cycles of RT-PCR were carried out for exon A/B and exon 5 of the *Zdbf2* gene (no SNPs were present) and *Actb* (as a control). (C) Quantitative RT-PCR analysis using the same primers as for (B) in ES cells and individual stage embryos. Expression levels of transcripts were normalized to those of the *Actb* gene. Error bars represent SEM ($n = 3$). (D) Allelic expression analysis of *Zdbf2* was performed using reciprocal F_1 hybrid embryos (B6 × JF and JF × B6), and embryos produced by mating between *Dnmt3L*-deficient females and JF males ($Dnmt3L^{mat-/-}$). Maternal and paternal alleles were distinguished by a SNP in exon A (C/T at chr1. 63,247,248; highlighted in yellow).

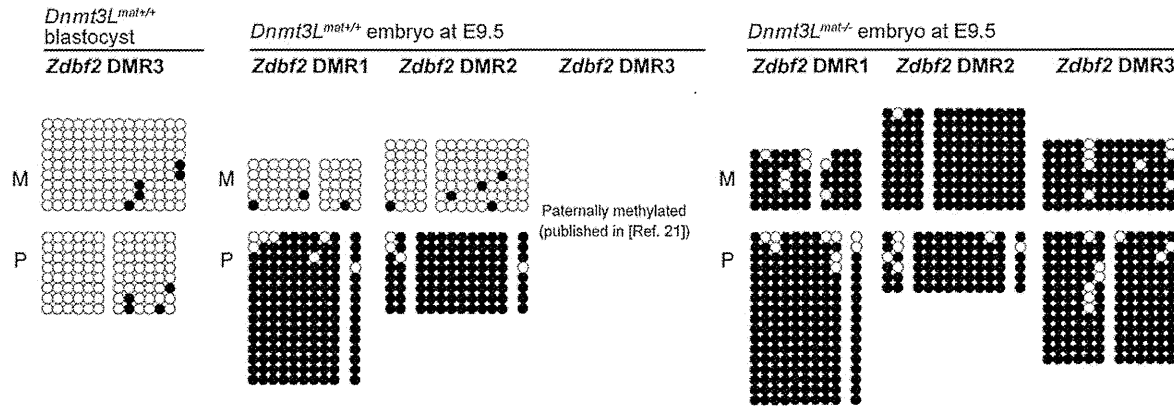

Fig. 4. DNA methylation profiles of the *Zdbf2* DMRs. Bisulfite sequencing analysis of *Zdbf2* DMR1, DMR2, and DMR3 in mouse embryos. M and P indicate the maternally inherited (B6 or 129 × B6) and paternally inherited (JF) alleles, respectively.

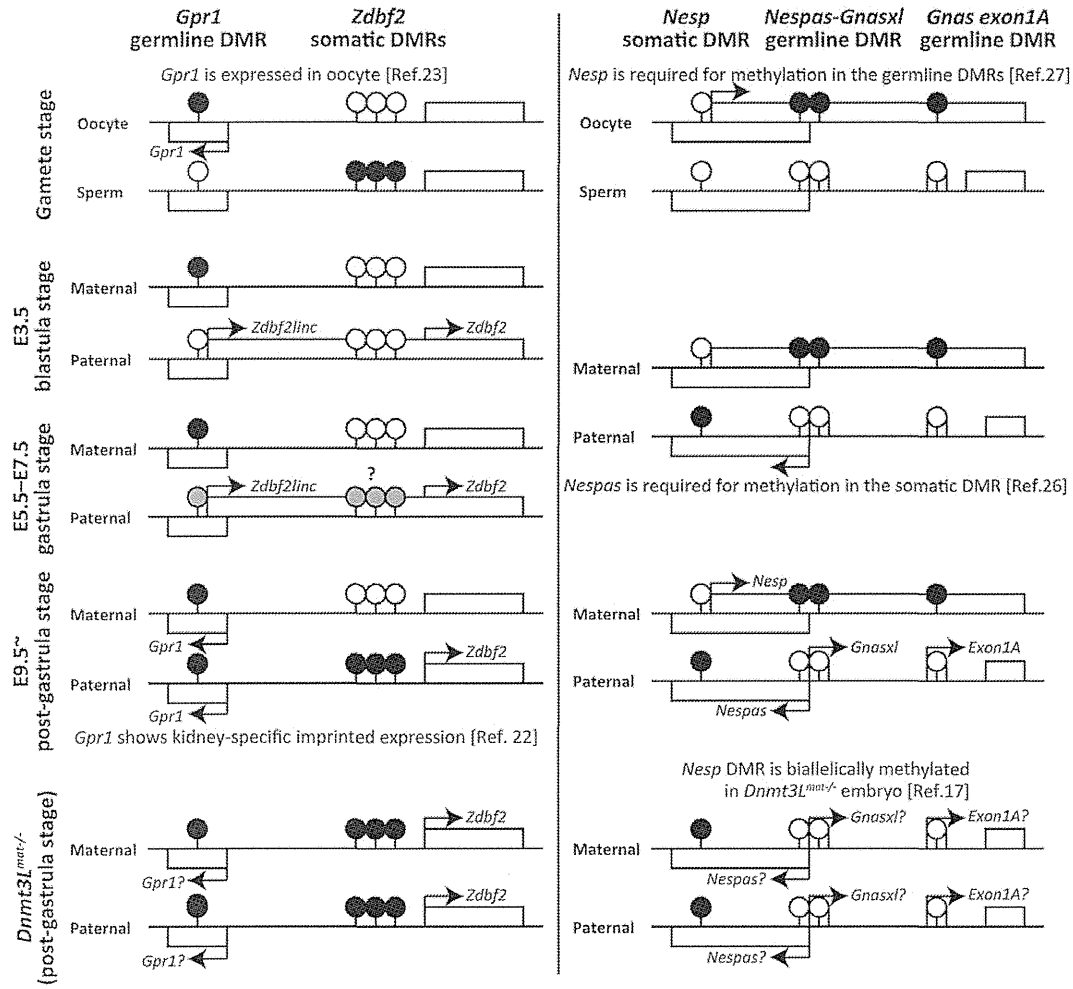

Fig. 5. Summary of allele-specific epigenetic and gene expression differences within the *Gpr1-Zdbf2* (left) and *Gnas* (right) loci. Open boxes represent the locations of the individual imprinted genes (or alternative promoter/first exons); arrows represent the transcriptional direction of these genes. The positions of the DMRs are indicated by filled and unfilled pins on the methylated and unmethylated alleles, respectively. Grey-filled pins indicate the partial methylated CpGs.

positively correlated to the expression of the original *Zdbf2* variant in *cis* after gastrulation.

4. Discussion

We identified a novel, long, imprinted, non-coding variant of the *Zdbf2* gene, *Zdbf2linc*, which is transcribed from the *Gpr1* DMR during the blastula and gastrula stages of mouse embryonic development. Furthermore, we found the paternal-allele-specific expression of *Zdbf2linc* to be negatively correlated with germline-derived maternal methylation at the *Gpr1* DMR. The *Gpr1* DMR was also shown to display complete biallelic methylation, while *Zdbf2linc* was rarely expressed in the post-gastrulation. It is unknown why the *Gpr1* DMR becomes hypermethylated after gastrulation; however, our results indicate that methylation at this DMR may repress the transcription of the *Zdbf2linc* variant in *cis*. The *Zdbf2* DMRs located within the transcribed region of *Zdbf2linc* were also shown to be secondary DMRs, with paternal-allele-specific methylation established after implantation. The imprinted *Gpr1-Zdbf2* locus therefore has two similarities with the *Gnas-Nespas*, *Kcnq1ot1*, and *Igf2r-Airn* imprinted clusters: (i) two differential states of imprinted methylation; namely, maternal-allele-specific methylation at gametogenesis and paternal-allele-specific methylation after fertilization, and (ii) transcription of long non-coding RNAs from each maternally methylated primary DMR (Fig. 5). Recently, lincRNAs have become a new paradigm for gene regulation via chromatin remodeling in a variety of biological processes, including events during embryonic development such as X chromosome dosage compensation [31,32], regulation of *Hox* genes [33], or genomic imprinting. The non-coding RNAs of the well-studied imprinted clusters *Nespas*, *Kcnq1ot1*, and *Airn* repress neighboring genes in *cis* [24–26], suggesting that the transcription of imprinted *Zdbf2linc* may also have a similar *cis*-regulating effect on flanking genes.

Allele-specific expression analyses using the heterozygous offspring of homozygous *Dnmt3L*-deficient females demonstrated that the imprinted expression of both *Zdbf2linc* and the original *Zdbf2* variant are subject to maternal methylation imprinting, whereby the original *Zdbf2* variant maintains paternal-allele-specific expression even after the gastrula stage, and *Zdbf2linc* and *Gpr1* DMR imprinting loss occurs. It is also possible that another mono-allelic epigenetic modification may become established via long-range transcription of *Zdbf2linc*, or that paternal-allele-specific methylation of *Zdbf2* DMRs may arise through the methylation of a transcribed region of *Zdbf2linc*. Some studies have also suggested that histone modifications at imprinted domains are a prerequisite for DNA methylation. Transcription across DMRs has been shown to be associated with histone methylation changes and the acquisition of genomic imprinting [26,27,34]. For example,

Williamson et al. have shown that paternally expressed non-coding *Nespas* transcription is required for the demethylation of trimethylated histone H3 lysine 4 (H3K4), followed by DNA methylation at the somatic *Nesp* DMR [26]. *Zdbf2linc* has also been identified as a lincRNA on the basis of the trimethylation states of H3K4 at its promoter region and histone H3 lysine 36 (H3K36) along its transcribed region, at least in ES cells [30]. Finally, the interaction of DNMT3A with chromatin is inhibited by H3K4 methylation [35], but promoted by H3K36 methylation [36]. Histone modifications may therefore control imprinted gene expression prior to allele-specific DNA methylation [5].

The imprinted *Gpr1-Zdbf2* locus also has features distinct from those of other imprinted loci. For instance, the primary *Gpr1* DMR does not maintain its mono-allelic methylation after fertilization, while the secondary *Zdbf2* DMRs are differentially methylated, even during gametogenesis. Furthermore, only paternally expressed transcripts were identified in the *Gpr1-Zdbf2* cluster, whereas the majority of imprinted clusters comprise both maternally and paternally expressed genes. Although the true functional roles of the *Gpr1* and *Zdbf2* genes remain unclear, we have herein identified a novel imprinted lincRNA variant of *Zdbf2* expressed exclusively from the paternal allele in the early embryo. Further investigations would elucidate the roles of the imprinted *Gpr1-Zdbf2* locus and its lincRNA variants in the control of embryonic growth and development.

Acknowledgment

This work was supported by Grants-in-Aid for Scientific Research from the Ministry of Education, Science, Sports and Culture of Japan (Grant Nos. 222228004, 20062009, 221S0002, S0801025).

References

[1] Reik, W. and Walter, J. (2001) Genomic imprinting: parental influence on the genome. Nat. Rev. Genet. 2, 21–32.
[2] Stoger, R., Kubicka, P., Liu, C.G., Kafri, T., Razin, A., Cedar, H. and Barlow, D.P. (1993) Maternal-specific methylation of the imprinted mouse Igf2r locus identifies the expressed locus as carrying the imprinting signal. Cell 73, 61–71.
[3] Coombes, C. et al. (2003) Epigenetic properties and identification of an imprint mark in the Nesp-Gnasxl domain of the mouse Gnas imprinted locus. Mol. Cell. Biol. 23, 5475–5488.
[4] Lopes, S. et al. (2003) Epigenetic modifications in an imprinting cluster are controlled by a hierarchy of DMRs suggesting long-range chromatin interactions. Hum. Mol. Genet. 12, 295–305.
[5] Bhogal, B., Arnaudo, A., Dymkowski, A., Best, A. and Davis, T.L. (2004) Methylation at mouse Cdkn1c is acquired during postimplantation development and functions to maintain imprinted expression. Genomics 84, 961–970.
[6] Sato, S., Yoshida, W., Soejima, H., Nakabayashi, K. and Hata, K. (2011) Methylation dynamics of IG-DMR and Gtl2-DMR during murine embryonic and placental development. Genomics 98, 120–127.
[7] Bourc'his, D., Xu, G.L., Lin, C.S., Bollman, B. and Bestor, T.H. (2001) Dnmt3L and the establishment of maternal genomic imprints. Science 294, 2536–2539.
[8] Hata, K., Okano, M., Lei, H. and Li, E. (2002) Dnmt3L cooperates with the Dnmt3 family of de novo DNA methyltransferases to establish maternal imprints in mice. Development 129, 1983–1993.
[9] Kaneda, M., Okano, M., Hata, K., Sado, T., Tsujimoto, N., Li, E. and Sasaki, H. (2004) Essential role for de novo DNA methyltransferase Dnmt3a in paternal and maternal imprinting. Nature 429, 900–903.
[10] Thorvaldsen, J.L., Duran, K.L. and Bartolomei, M.S. (1998) Deletion of the H19 differentially methylated domain results in loss of imprinted expression of H19 and Igf2. Genes Dev. 12, 3693–3702.
[11] Bielinska, B., Blaydes, S.M., Buiting, K., Yang, T., Krajewska-Walasek, M., Horsthemke, B. and Brannan, C.I. (2000) De novo deletions of SNRPN exon 1 in early human and mouse embryos result in a paternal to maternal imprint switch. Nat. Genet. 25, 74–78.
[12] Wutz, A., Theussl, H.C., Dausman, J., Jaenisch, R., Barlow, D.P. and Wagner, E.F. (2001) Non-imprinted Igf2r expression decreases growth and rescues the Tme mutation in mice. Development 128, 1881–1887.
[13] Fitzpatrick, G.V., Soloway, P.D. and Higgins, M.J. (2002) Regional loss of imprinting and growth deficiency in mice with a targeted deletion of KvDMR1. Nat. Genet. 32, 426–431.
[14] Yoon, B.J., Herman, H., Sikora, A., Smith, L.T., Plass, C. and Soloway, P.D. (2002) Regulation of DNA methylation of Rasgrf1. Nat. Genet. 30, 92–96.
[15] Lin, S.P., Youngson, N., Takada, S., Seitz, H., Reik, W., Paulsen, M., Cavaille, J. and Ferguson-Smith, A.C. (2003) Asymmetric regulation of imprinting on the maternal and paternal chromosomes at the Dlk1-Gtl2 imprinted cluster on mouse chromosome 12. Nat. Genet. 35, 97–102.
[16] Williamson, C.M. et al. (2004) A cis-acting control region is required exclusively for the tissue-specific imprinting of Gnas. Nat. Genet. 36, 894–899.
[17] Liu, J., Chen, M., Deng, C., Bourc'his, D., Nealon, J.G., Erlichman, B., Bestor, T.H. and Weinstein, L.S. (2005) Identification of the control region for tissue-specific imprinting of the stimulatory G protein alpha-subunit. Proc. Natl. Acad. Sci. USA 102, 5513–5518.
[18] Williamson, C.M. et al. (2006) Identification of an imprinting control region affecting the expression of all transcripts in the Gnas cluster. Nat. Genet. 38, 350–355.
[19] Shiura, H. et al. (2009) Paternal deletion of Meg1/Grb10 DMR causes maternalization of the Meg1/Grb10 cluster in mouse proximal chromosome 11 leading to severe pre- and postnatal growth retardation. Hum. Mol. Genet. 18, 1424–1438.
[20] Babak, T., Deveale, B., Armour, C., Raymond, C., Cleary, M.A., van der Kooy, D., Johnson, J.M. and Lim, L.P. (2008) Global survey of genomic imprinting by transcriptome sequencing. Curr. Biol. 18, 1735–1741.
[21] Kobayashi, H. et al. (2009) Identification of the mouse paternally expressed imprinted gene Zdbf2 on chromosome 1 and its imprinted human homolog ZDBF2 on chromosome 2. Genomics 93, 461–472.
[22] Hiura, H. et al. (2010) A tripartite paternally methylated region within the Gpr1-Zdbf2 imprinted domain on mouse chromosome 1 identified by meDIP-on-chip. Nucleic Acids Res. 38, 4929–4945.
[23] Kobayashi, H. et al. (2012) Contribution of intragenic DNA methylation in mouse gametic DNA methylomes to establish oocyte-specific heritable marks. PLoS Genet. 8, e1002440.
[24] Sleutels, F., Zwart, R. and Barlow, D.P. (2002) The non-coding Air RNA is required for silencing autosomal imprinted genes. Nature 415, 810–813.
[25] Mancini-Dinardo, D., Steele, S.J., Levorse, J.M., Ingram, R.S. and Tilghman, S.M. (2006) Elongation of the Kcnq1ot1 transcript is required for genomic imprinting of neighboring genes. Genes Dev. 20, 1268–1282.
[26] Williamson, C.M. et al. (2011) Uncoupling antisense-mediated silencing and DNA methylation in the imprinted Gnas cluster. PLoS Genet. 7, e1001347.
[27] Chotalia, M. et al. (2009) Transcription is required for establishment of germline methylation marks at imprinted genes. Genes Dev. 23, 105–117.
[28] Arnaud, P., Hata, K., Kaneda, M., Li, E., Sasaki, H., Feil, R. and Kelsey, G. (2006) Stochastic imprinting in the progeny of Dnmt3L−/− females. Hum. Mol. Genet. 15, 589–598.
[29] Kumaki, Y., Oda, M. and Okano, M. (2008) QUMA: quantification tool for methylation analysis. Nucleic Acids Res. 36, W170–W175.
[30] Guttman, M. et al. (2010) Ab initio reconstruction of cell type-specific transcriptomes in mouse reveals the conserved multi-exonic structure of lincRNAs. Nat. Biotechnol. 28, 503–510.
[31] Ohhata, T., Senner, C.E., Hemberger, M. and Wutz, A. (2011) Lineage-specific function of the noncoding Tsix RNA for Xist repression and Xi reactivation in mice. Genes Dev. 25, 1702–1715.
[32] Ng, K., Pullirsch, D., Leeb, M. and Wutz, A. (2007) Xist and the order of silencing. EMBO Rep. 8, 34–39.
[33] Rinn, J.L. et al. (2007) Functional demarcation of active and silent chromatin domains in human HOX loci by noncoding RNAs. Cell 129, 1311–1323.
[34] Henckel, A., Chebli, K., Kota, S.K., Arnaud, P. and Feil, R. (2012) Transcription and histone methylation changes correlate with imprint acquisition in male germ cells. EMBO J. 31, 606–615.
[35] Zhang, Y. et al. (2010) Chromatin methylation activity of Dnmt3a and Dnmt3a/3L is guided by interaction of the ADD domain with the histone H3 tail. Nucleic Acids Res. 38, 4246–4253.
[36] Dhayalan, A., Rajavelu, A., Rathert, P., Tamas, R., Jurkowska, R.Z., Ragozin, S. and Jeltsch, A. (2010) The Dnmt3a PWWP domain reads histone 3 lysine 36 trimethylation and guides DNA methylation. J. Biol. Chem. 285, 26114–26120.

Contribution of Intragenic DNA Methylation in Mouse Gametic DNA Methylomes to Establish Oocyte-Specific Heritable Marks

Hisato Kobayashi[1], Takayuki Sakurai[1], Misaki Imai[2], Nozomi Takahashi[1], Atsushi Fukuda[1], Obata Yayoi[1], Shun Sato[3], Kazuhiko Nakabayashi[3], Kenichiro Hata[3], Yusuke Sotomaru[4], Yutaka Suzuki[5], Tomohiro Kono[1,2]*

1 Department of BioScience, Tokyo University of Agriculture, Tokyo, Japan, **2** Genome Research Center, NODAI Research Institute, Tokyo University of Agriculture, Tokyo, Japan, **3** Department of Maternal-Fetal Biology, National Research Institute for Child Health and Development, Tokyo, Japan, **4** Natural Science Center for Basic Research and Development, Hiroshima University, Hiroshima, Japan, **5** Department of Medical Genome Sciences, Graduate School of Frontier, The University of Tokyo, Kashiwa, Japan

Abstract

Genome-wide dynamic changes in DNA methylation are indispensable for germline development and genomic imprinting in mammals. Here, we report single-base resolution DNA methylome and transcriptome maps of mouse germ cells, generated using whole-genome shotgun bisulfite sequencing and cDNA sequencing (mRNA-seq). Oocyte genomes showed a significant positive correlation between mRNA transcript levels and methylation of the transcribed region. Sperm genomes had nearly complete coverage of methylation, except in the CpG-rich regions, and showed a significant negative correlation between gene expression and promoter methylation. Thus, these methylome maps revealed that oocytes and sperms are widely different in the extent and distribution of DNA methylation. Furthermore, a comparison of oocyte and sperm methylomes identified more than 1,600 CpG islands differentially methylated in oocytes and sperm (germline differentially methylated regions, gDMRs), in addition to the known imprinting control regions (ICRs). About half of these differentially methylated DNA sequences appear to be at least partially resistant to the global DNA demethylation that occurs during preimplantation development. In the absence of *Dnmt3L*, neither methylation of most oocyte-methylated gDMRs nor intragenic methylation was observed. There was also genome-wide hypomethylation, and partial methylation at particular retrotransposons, while maintaining global gene expression, in oocytes. Along with the identification of the many *Dnmt3L*-dependent gDMRs at intragenic regions, the present results suggest that oocyte methylation can be divided into 2 types: *Dnmt3L*-dependent methylation, which is required for maternal methylation imprinting, and *Dnmt3L*-independent methylation, which might be essential for endogenous retroviral DNA silencing. The present data provide entirely new perspectives on the evaluation of epigenetic markers in germline cells.

Citation: Kobayashi H, Sakurai T, Imai M, Takahashi N, Fukuda A, et al. (2012) Contribution of Intragenic DNA Methylation in Mouse Gametic DNA Methylomes to Establish Oocyte-Specific Heritable Marks. PLoS Genet 8(1): e1002440. doi:10.1371/journal.pgen.1002440

Editor: Wolf Reik, The Babraham Institute, United Kingdom

Received July 28, 2011; **Accepted** November 14, 2011; **Published** January 5, 2012

Copyright: © 2012 Kobayashi et al. This is an open-access article distributed under the terms of the Creative Commons Attribution License, which permits unrestricted use, distribution, and reproduction in any medium, provided the original author and source are credited.

Funding: This work was supported by Grants-in-Aid for Scientific Research from the Ministry of Education, Science, Sports, and Culture of Japan (Grant Nos. 222228004, 20062009, 221S0002, S0801025). The funders had no role in study design, data collection and analysis, decision to publish, or preparation of the manuscript.

Competing Interests: The authors have declared that no competing interests exist.

* E-mail: tomohiro@nodai.ac.jp

Introduction

Throughout mammalian gametogenesis, dynamic DNA methylation changes occur in a sex- and sequence-specific manner. These changes result in the establishment of oocyte- and sperm-specific genomic imprints and unique methylation patterns of repetitive elements via DNA methyltransferase activity [1–4]. This process is indispensable for functional gamete and embryo development. For example, sex-specific methylation imprints are maintained throughout cell division after fertilization, despite genome-wide demethylation and *de novo* methylation during embryogenesis. These imprints control parent-of-origin specific monoallelic expression of a subset of genes, which are known as imprinted genes [5–9]. In addition, DNA methylation during spermatogenesis plays a crucial role in meiotic progression and retrotransposon silencing [10–14]. However, little is known about the profile and functional role of DNA methylation during oogenesis, except for the establishment of genomic imprints.

Recently, the epigenetic modifications which are responsible for regulating cell differentiation and embryo development have been studied in detail by using high-throughput sequencing: bisulfite sequencing ("BS-seq"); "Methyl-seq" with a methyl-sensitive restriction enzyme; "MeDIP-seq" with methylated DNA immunoprecipitation; and "MBD-seq" with a methyl-DNA binding domain protein antibody [15–26]. However, a major limitation of epigenomic studies is the lack of a standard methodology for DNA methylome analysis. Ideally, the gold standard is high resolution and genome-wide methylome analysis of germ cells. However, genome-wide methylome analysis of female germ cells has almost never been performed due to the limited availability of samples.

Author Summary

In mammals, germ-cell–specific methylation patterns and genomic imprints are established throughout large-scale de novo DNA methylation in oogenesis and spermatogenesis. These steps are required for normal germline differentiation and embryonic development; however, current DNA methylation analyses only provide us a partial picture of germ cell methylome. To the best of our knowledge, this is the first study to generate comprehensive maps of DNA methylomes and transcriptomes at single base resolution for mouse germ cells. These methylome maps revealed genome-wide opposing DNA methylation patterns and differential correlation between methylation and gene expression levels in oocyte and sperm genomes. In addition, our results indicate the presence of 2 types of methylation patterns in the oocytes: (i) methylation across the transcribed regions, which might be required for the establishment of maternal methylation imprints and normal embryogenesis, and (ii) retroviral methylation, which might be essential for silencing of retrotransposons and normal oogenesis. We believe that an extension of this work would lead to a better understanding of the epigenetic reprogramming in germline cells and of the role for gene regulations.

Shotgun bisulfite sequencing (SBS) may be able to overcome this limitation and enable the determination of the cytosine methylation status of individual CpG sites at a whole-genome level without a bias toward CpG-rich regions [22,23,26] and with only relatively small-scale DNA samples [24,27]. As a result, in this study, an improved SBS method for small-scale DNA samples was used to analyze the DNA methylome of mouse germ cells. In addition, the mouse germ cell transcriptome was investigated using high-throughput cDNA sequencing (mRNA-seq) to reveal relationships between DNA methylation and gene transcription in both male and female germ cells.

Results

Genome sequencing

We performed SBS analysis by using MethylC-seq [22] and a new SBS method called "whole bisulfitome-amplified DNA sequencing" (WBA-seq). The MethylC-seq and WBA-seq libraries were generated as shown in Figure S1. The MethylC-seq method generated 1010 and 1085 million tags (reads) from germinal vesicle (GV) stage oocytes and epididymal sperm, respectively. Oocyte DNA libraries generated by MethylC-seq showed higher redundancies than sperm DNA libraries. For example, 33.0% and 81.7% of the 21 million cytosines of CpGs in the mouse genome were covered by at least 1 sequence read from GV oocytes and sperm, respectively; whereas the average read depth (*i.e.*, the number of hits of reads that were mapped to a given position) was over 10× for both germ cells (Figure S2). The WBA-seq method generated 307 and 397 million tags from GV oocytes obtained from wild-type and *Dnmt3L*-deficient (*Dnmt3L*$^{-/-}$) mice, respectively. WBA-seq libraries for GV oocytes showed higher genome coverage (60% of genomic CpGs were covered by at least 1 read) but with smaller average read depth (7.4×) than MethylC-seq library. Some reads from the oocyte libraries strongly matched mitochondrial DNA (mtDNA), satellite, low complexity, or simple repeat sequences (Figure S3), which might have been due to a distinct genomic copy number bias in the mitochondria of germ cells or an over-amplification bias. Thus, SBS results were simplified by removing the redundancy information (only mtDNA was separately examined for DNA methylation) and combining MethylC-seq and WBA-seq results for wild-type oocytes. Consequently, the average read depth was 18.8×, 4.4×, and 12.5× for wild-type and *Dnmt3L*$^{-/-}$ oocytes, and sperm, respectively, and 70.8%, 45.6%, and 79.9% of genomic CpGs were covered by at least 1 sequence read from each cell type (Table 1 and Figure S3). Furthermore, the average read depths of MethylC-seq of mouse blastocysts and embryonic stem cells (ESCs), which served as zygote and stem cell controls, were 12.8× and 6.1×, respectively (Table 1).

Methylome of mouse germ cells

The average methylation level of wild-type oocytes (40.0%) was less than half that of sperm (89.4%) (Figure S4). This difference in global DNA methylation between male and female germ cells was consistent with results from the previous studies [28,29]. The *Dnmt3L*$^{-/-}$ oocyte genome was observed to be hypomethylated, exhibiting a methylation level of only 5.5%. Furthermore, blastocysts showed a lesser extent of methylation (21.3%) than did wild-type oocytes; ESCs, on the other hand, showed relatively high levels of methylation (70.6%). To elucidate the distribution of methylation levels on CpG sites, on regional and genome-wide scales, we created dot plots of CpG methylation for individual chromosomes and histograms of the methylation levels for all CpGs. These graphs revealed that hypermethylated CpGs in oocytes tended to cluster in transcribed regions of particular genes (*e.g.*, *Kcnq1* or *Rlim* genes, known to be expressed in oocytes [30,31]); the sperm genome was almost entirely hypermethylated, except at most CpG-rich regions (Figure 1 and Figure S5). Specifically, 55.7% of the CpGs in the oocyte genome exhibited <10% methylation, whereas another 32.0% of CpGs exhibited ≥90% methylation (Figure 2A). The *Dnmt3L*$^{-/-}$ oocyte genome was also hypomethylated in almost all chromosomal regions (Figure S6). The methylation level of the mtDNA genome in

Table 1. Summary of shotgun bisulfite sequencing data.

Sample	Method	Aligned tags (base)	Genome covarage		Read depth
			(>x1)	(>x5)	
Wild-type oocyte	MethylC-seq & WBA-seq	51,166,451,066	70.8%	39.4%	18.8
Dnmt3L$^{-/-}$ oocyte	WBA-seq	11,872,662,647	45.6%	19.6%	4.4
Sperm	MethylC-seq	34,153,237,944	79.9%	63.4%	12.5
Blastocyst	MethylC-seq	34,857,014,339	86.2%	79.4%	12.8
ESC	MethylC-seq	16,691,289,063	73.0%	38.9%	6.1

doi:10.1371/journal.pgen.1002440.t001

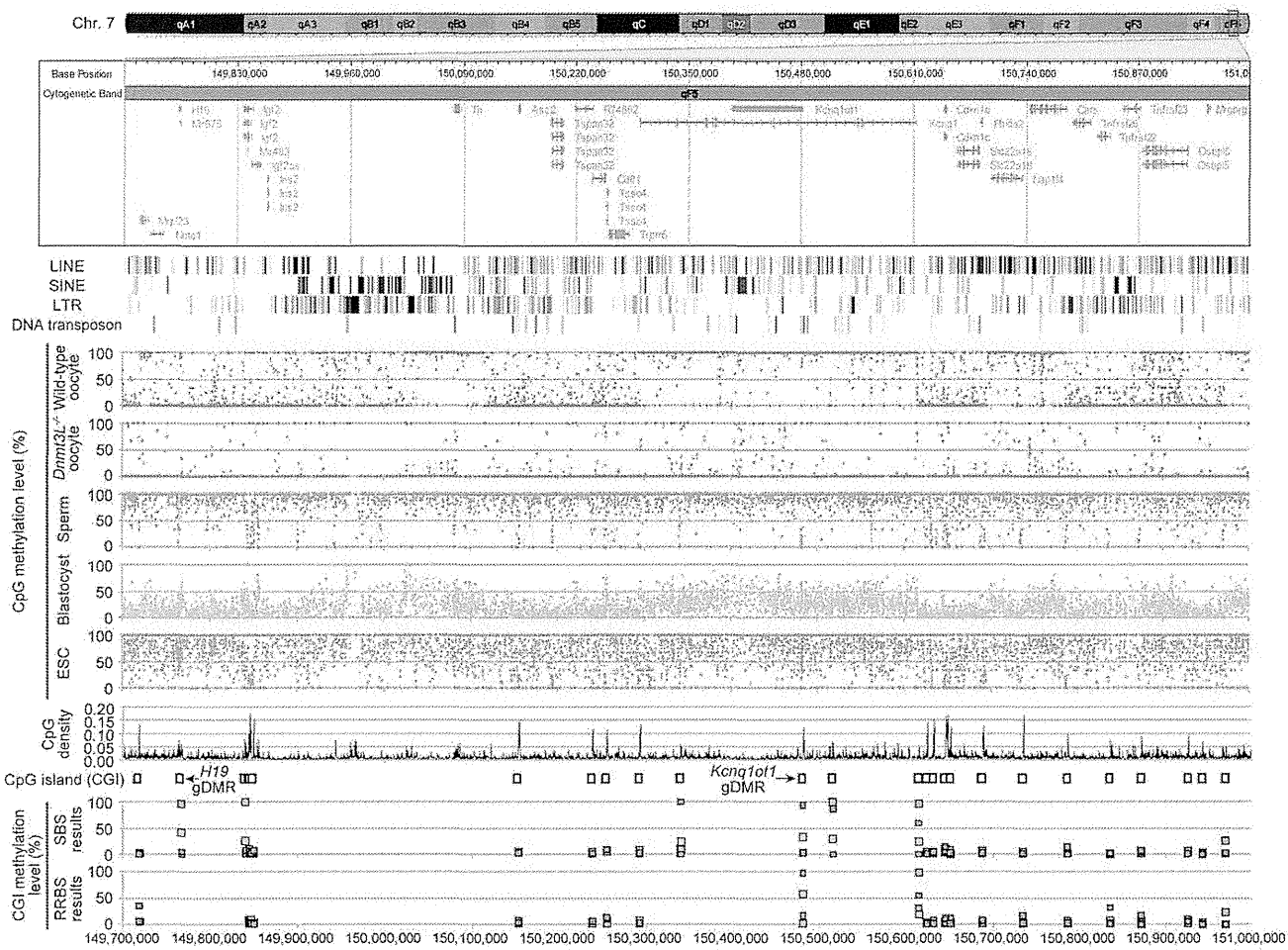

Figure 1. High-resolution DNA methylome map of mouse distal chromosome 7 imprinting cluster. Illumina GenomeStudio viewer displays the locations of genes in distal chromosome 7 (149,700,000–151,000,000). Black vertical bars represent the location of 4 repetitive elements: LINE, SINE, LTR, and DNA transposons. Red, purple, blue, green, and khaki dots represent the methylation levels at individual CpGs in wild-type oocyte, *Dnmt3L*$^{-/-}$ oocyte, sperm, blastocyst, and ESC genomes, respectively. Black line plots depict the distribution of CpG densities (number of CpG per 200 nt) of individual CpGs. Open boxes represent the location of CpG islands (CGIs). Red, purple, blue, and green boxes represent the methylation levels at individual CGIs in wild-type oocyte, *Dnmt3L*$^{-/-}$ oocyte, sperm, and blastocyst genomes, respectively, determined by our results from shotgun bisulfite sequencing (SBS) method and Smallwood's results from reduced representation bisulfite sequencing (RRBS) method [38].
doi:10.1371/journal.pgen.1002440.g001

Dnmt3L$^{-/-}$ oocytes (4.4%) was lower than that observed in wild-type oocytes (6.6%). Sperm methylation levels, by comparison, were relatively high (14.7%), whereas those of the blastocysts and ESCs were quite low (1.3% and 2.1%, respectively) (Figure S4).

Since previous studies revealed a significant correlation between CpG frequency and methylation within intra- and intergenic regions in somatic cells [32,33], the CpG density and methylation levels were compared to identify genome-wide differential methylation patterns in germ cells. CpG density was defined as the number of CpG dinucleotides in 200 nucleotide (nt) windows (*e.g.*, 1 CpG dinucleotide per 200 nt corresponds to a density of 0.005). At low CpG densities (range, 0.005–0.05), the oocyte genome was about 50% methylated, whereas the sperm genome was 80–90% methylated. At moderate to high CpG densities (range, 0.05–0.2), both male and female germ cells were hypomethylated (Figure 2B). Furthermore, 4 families of transposable elements (long interspersed nuclear elements (LINEs), short interspersed nuclear elements (SINEs), long terminal repeats (LTRs), and DNA transposons) were moderately methylated in oocyte genomes but were hypermethylated in sperm. In addition, a general trend towards higher methylation levels at higher CpG densities in the oocyte genome occurred in LTRs. Conversely, a trend toward lower CpG methylation levels at higher CpG densities in the wild-type oocyte and sperm genomes was observed in SINEs and DNA transposons. In contrast, all of these transposable elements were hypomethylated in *Dnmt3L*$^{-/-}$ oocytes. Interestingly, however, there was partial CpG methylation in LINEs and LTRs at relatively high CpG densities (range, 0.03–0.1). These complete or partial under-methylations were confirmed by bisulfite sequencing in L1 LINEs, B1/Alu SINEs, and intracisternal A particle (IAP) LTRs (Figure S7). These results suggested that each germ cell has a unique sequence- and CpG-density-dependent methylation pattern. In addition, oocyte CpG methylation, except in a subset of retrotransposons, appears to be *Dnmt3L* dependent.

We also characterized the methylation patterns of 15 germline-differentially methylated regions (gDMRs). The differential (between oocyte and sperm) methylation occurs at imprinted gene loci (also called imprinting control regions (ICRs)). The ICRs of maternally methylated imprinted genes (*e.g.*, *Nespas-Gnas*) were shown to be hypermethylated in oocytes but hypomethylated in sperm, while the converse was true in ICRs of paternally-methylated imprinted genes (*e.g.*, *H19*) (Figure 3 and Figure S8). Interestingly, only the *Snrpn*

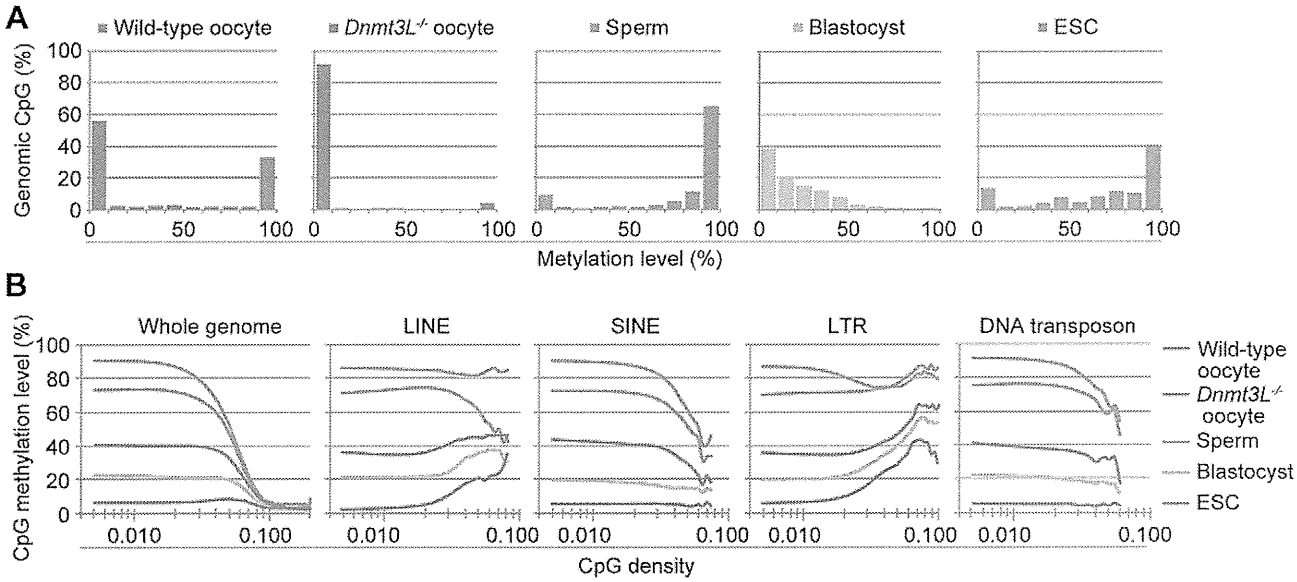

Figure 2. Genome-wide methylation profiling of mouse germ cells. (A) Histograms of methylation levels of genomic CpGs in wild-type oocyte, *Dnmt3L*$^{-/-}$ oocyte, sperm, blastocyst, and embryonic stem cell (ESC) genomes. (B) CpG methylation levels are plotted as a function of CpG density for the whole genome and 4 families of transposable elements (long interspersed nuclear element (LINE), short interspersed nuclear element (SINE), long terminal repeat (LTR), and DNA transposon).
doi:10.1371/journal.pgen.1002440.g002

gDMR was partially methylated (35.7%), whereas all other maternal ICRs were hypomethylated in *Dnmt3L*$^{-/-}$ oocytes (Table 2). This residual methylation might result in the stochastic acquisition of the maternal imprint in the progeny of *Dnmt3L*$^{-/-}$ females [34]. These results strongly suggested that the methylation level of individual CpGs can be determined from DNA methylome maps with a high degree of accuracy.

The study of mammalian DNA methylation patterns has previously suggested that methylation predominantly occurs at CpG sites; however, more recent studies, based on SBS methods, have indicated that methylation at non-CpG sites also occurs in human ESCs [22,23]. Detection of non-CpG methylation is one of the applications of the bisulfite-based methylation analysis but is problematic due to the incomplete conversion of cytosine, and overestimates of such cytosine by PCR amplification, which cannot be discriminated from true methylation. In order to evaluate the methylation status of non-CpG sites and avoid these problems, additional SBS analysis of mouse GV oocytes, sperm, blastocysts, and ESCs was performed by a non-amplification technique, termed Post-Bisulfite Adapter Tagging (PBAT) [Miura F. & Ito T, personal communication]. All C (originally methylated cytosine) and T (originally unmethylated cytosine) that mapped to genomic CpG and CpH sites (H = A, T, or C) were counted. The PBAT results showed CpG methylation ratios (C ratios = 0.395, 0.748, 0.137, 0.615 in oocytes, sperm. blastocysts, and ESCs) which are similar to the average methylation levels of individual DNA methylome maps obtained by MethylC-seq and WBA-seq among all examined cells. Interestingly, a relatively high fold enrichment of non-CpG methylation was observed in GV oocytes (C ratio = 0.034–0.038), but not in the other cell types, including mouse ESCs (C ratio <0.01) (Figure S11).

Relationship between the DNA methylome and transcriptome of mouse germ cells

To elucidate the interaction between intragenic DNA methylation and gene transcription, the correlation between promoter and gene-body methylation and expression levels for 20,854 different genes was examined. The mRNA-seq profiles for germ cells and ESCs are shown in Table S1. The results showed that mRNA transcript levels in oocytes were strongly correlated to gene-body methylation levels (Spearman's $\rho > 0.5$, $p < 1 \times 10^{-9}$) but were not significantly correlated to promoter methylation levels ($|\rho| < 0.1$) (Figure 4A). For example, the regions +2 to +5 kb from the transcription start site (TSS) and 0 to −5 kb from the transcription termination site (TTS) were hypermethylated (60–90% methylation) for the top 20% of expressed genes but were hypomethylated (10–30% methylation) for the bottom 20% of expressed genes. However, areas near the TSS (±500 base pairs (bp)) were hypomethylated (10–20% methylation) in all genes, regardless of their expression level. In contrast, in the *Dnmt3L*$^{-/-}$ oocyte genome, the correlation between gene expression and gene-body methylation was very weak ($|\rho| < 0.1$) (Figure 4B). In the sperm genome, promoter methylation was negatively correlated (Spearman's $\rho = -0.36$, $p < 1 \times 10^{-9}$) with gene expression, whereas gene-body methylation was positively correlated (Spearman's $\rho = 0.14$–0.16, $p < 1 \times 10^{-9}$) to gene expression; the latter correlation was weaker than that observed in the oocyte genome (Figure 4C).

Role of *Dnmt3L* in the DNA methylome/transcriptome relationship

Further investigation of gene expression patterns in oocyte genomes revealed that the mRNA transcript levels between wild-type and *Dnmt3L*$^{-/-}$ oocytes were very highly correlated ($R^2 = 0.9611$) (Figure 5A). In fact, there were no significant differences in the expression levels of representative oocyte-specific genes (*e.g.*, *Gdf9*, *Bmp15*, *Bcl2l10*, *Zp1*, *Zp2*, *Zp3*, *Zar1*, *Npm2*, *Nlrp5*, and *Dppa3*, which are responsible for ovarian follicle formation, reproduction, and early development [35]) and DNA methyltransferase genes (*e.g.*, *Dnmt1*, a maintenance methyltransferase, and *Dnmt3a* and *Dnmt3b de novo* methyltransferases); the expected difference in the expression level of *Dnmt3L* between wild-type and